UNIZIK JOURNAL OF ENGINEERING AND APPLIED SCIENCES (UJEAS)

Research Article

Kinetic and Modeling of Anionic Dye Adsorption onto Acid modified Ihiala Clays: ANN, ANFIS and RSM comparative analysis

Nonso C. Oguanobi, George Okonkwo, Okechukwu D. Onukwuli, Calistus N. Ude, Ephrem N. Anike

Special Issue
A Themed Issue in Honour of Professor Clement Uche Atuanya on His retirement.

This themed issue pays tribute to Professor Clement Uche Atuanya in recognition of his illustrious career in Metallurgical and Materials Engineering as he retires from Nnamdi Azikiwe University, Awka. We celebrate his enduring legacy of dedication to advancing knowledge and his impact on academia and beyond through this collection of writings.

Edited by
Chinonso Hubert Achebe PhD.
Christian Emeka Okafor PhD.

UJEAS

UNIZIK JOURNAL OF ENGINEERING AND APPLIED SCIENCES

UNIZIK Journal of Engineering and Applied Sciences 3(3), September (2024), 867-902
Journal homepage: https://journals.unizik.edu.ng/index.php/ujeas
PRINT ISSN: 2992-4383 || ONLINE ISSN: 2992-4391

Kinetic and Modeling of Anionic Dye Adsorption onto Acid modified Ihiala Clays: ANN, ANFIS and RSM comparative analysis

Nonso C. Oguanobi[1]*, George Okonkwo[1], Okechukwu D. Onukwuli[2], Calistus N. Ude[1], Ephrem N. Anike[1].

[1.] Department of Chemical Engineering, Michael Okpara University of Agriculture, Umudike, Abia State, Nigeria.

[2.] Department of Chemical Engineering, Nnamdi Azikiwe University, Awka, Nigeria

*****Corresponding Author's E-mail: oguanobi.nonso@mouau.edu.ng.

Abstract

Congo red (CR) dye is a harmful dye of environmental concern due to its complex molecular structure and artificial origin, which make it non-biodegradable. The research focused on using the physico-chemical method to remove CR pollutants (color, dissolved salt (EC), total dissolved solids (TDS), and chemical oxygen demand (COD)) from effluent by utilizing the adsorptive qualities of acid-modified Ihiala clay (HIC). The batch system was applied to evaluate the effect of process-independent variables on the adsorption process. The mechanism of adsorption was investigated using intra-particle diffusion, liquid film, the Bangham model, and the Boyd model. The thermodynamic properties ΔS, ΔH, ΔG, and ΔEa were determined. The optimum removal efficiency of CR was predicted using the ANN, ANFIS, and RSM models. The activation resulted in an increase in surface area. Maximum color removal of 99.3% was observed at pH 2, an adsorbent dosage of 1 g, an adsorbent particle size of 75 µm, an initial dye concentration of 100 mg/l, a contact time of 120 min, and a temperature of 323 k. A maximum adsorption capacity of 86.70 mg/g was obtained. The liquid film diffusion was the major rate-limiting step. Thermodynamic results suggested an endothermic, favorable, spontaneous, and physical adsorption process. The RSM model is statistically more significant than the ANFIS and ANN models. A maximum desorption capacity of 90.3% was achieved after four cycles. The obtained results confirm HIC as a reliable, cost-effective adsorbent for CR pollutants removal from effluents.

Keywords: adsorption; kinetics; modeling; thermodynamics; artificial neural networks.

1. Introduction

Environmental contamination has been one of the greatest challenges of mechanized society, mainly due to the dense population and its increasing demand, which leads to increased industrial activity. The high degree of industrialization in the world has resulted in different forms of pollution. Water pollution has been a matter of public concern because it can affect both mankind and the ecological balance of ecosystems. Water pollution arises as a result of discharging into the water body's untreated industrial effluent, dumping of untreated industrial waste, human waste or garbage, and dead animals into waterways, oil leaks and spills, agricultural runoff, etc. Industrial wastewater contains 60% of the total pollutants in water bodies. Most pollutants in industrial effluent are generated from industries such as textile, tanning, heavy metal (lead, mercury, copper, and nickel) factories, paints, paper, rubber, cement, glass, leather, detergents, pharmaceuticals, dairy sterilization plants, food, slaughterhouses, cosmetic sugar refineries, dye production, oil industries, etc. Industrial effluent contains a large amount of dissolved dyestuffs and other products such as dispersing agents, dye bath carriers, salts, emulsifiers, leveling agents, oil, and heavy metals (Noroozi *et al.* 2007).

The oil refining process industries and dye production and consumption industries are the major contributors to the total industrial wastewater pollution in water bodies. Among the many sources of industrial dye wastewater are textile, rubber, leather, paper and pulp, plastic, soap and detergent, food, paint, petrochemical, photographic, printing ink, pharmaceutical, cosmetics, mills, and mining operations. The high rate of water pollution is linked to poor waste

management and a lack of strict laws regulating the discharge of sewage or inadequately treated effluents into the environment. This results in the discharge of sewage from industries into the environment without proper treatment. Recently, different physical, biological, physico-chemical, and chemical treatment techniques such as coagulation and flocculation, sonochemical degradation, adsorption, photochemical degradation, electrochemical removal, electrochemical degradation, membrane separation, bio-degradation, anaerobic sequential process Fenton-biological treatment scheme, photo-Fenton process, and oxidation and zonation have been explored in trying to minimize the trait of water pollution from the point source. All of these treatment techniques, except adsorption, have certain limitations and haven't been able to completely remove the color from wastewater (Oguanobi *et al.* 2019).

Adsorption is a unit operation and a mass transfer operation process that involves the adhesion of molecules, ions, and atoms from a liquid, dissolved solid, or gas to the surface of a material called an adsorbent. Therefore, an adsorbent is any material that is capable of removing dissolved components from an aqueous solution through the force of attraction that exits between the aqueous solution (adsorbate) and the surface of the adsorbent. This unit operation process finds great use in many industrial applications where water recovery is essential, such as textile, rubber, leather, paper and pulp, plastic, soap and detergent, food, paint, petrochemical, photographic, printing ink, pharmaceuticals, cosmetics, etc. Activated carbon has been the conventional adsorbent for the adsorption process over time due to its uniqueness and high adsorption capacity, but the limitation of high operating costs becomes a serious concern and thereby raises the quest for a non-conventional, low-cost alternative. Different non-conventional adsorbents have been exploited, and all show the capacity to replace conventional activated carbon. Some of the previously exploited non-conventional adsorbents include modified clays (Oguanobi *et al.* 2019, Nayoon *et al.* 2022), modified biomass (Mohammed *et al.* 2023), red clay (Muhammed and Çiğdem 2022), eggplant biomass (Zhi *et al.* 2022), black stone cherries (Arana and Mazzoco 2010), agriculture waste (Dal and Meenal 2022), neem leaf powder (Bhattacharyya and Sharma 2005), rice hull (El-Halwany 2010), rice bran (Mojtaba *et al.* 2020), and rice husk (Onu *et al.* 2020), clay mineral (Juraj 2023, Zineb *et al.* 2023, Mohammed *et al.* 2022), zeolite-based bio-membrane (Sabarish *et al.* 2022), among others.

However, among all these exploited adsorbents, clays exhibit high adsorption capacity due to their ability to adsorb ions and molecules on both external and interlayer particle sites. Adsorption and desorption of organic molecules in clays are controlled by the surface properties of the clay, such as its large surface area, low permeability, high retention, and cation exchange capacities. Natural clay exhibits a negative charge of structure, which allows it to adsorb positively charged dyes but induces a low adsorption capacity for anionic dyes (Mahammedi and Benguella 2016). The natural high adsorption strengths of clay can be further enhanced through modification. Modification of clay creates a positive-charged structure, which also allows the adsorption of anionic dyes (negatively charged dyes). Most works on CR dye removal have focused on studying the influence of these factors using the one-factor-at-a-time method, which is cumbersome, time-consuming, and cannot satisfactorily predict the optimum point of process variables.

Response surface methodology (RSM) is a model used to generate a mathematical model that can satisfactorily give the optimum parameters for operating a process. It helps in the simultaneous examination of process variables that affect a process, even in the presence of complex interactions. RSM only needs small experimental runs to predict an optimum condition. Artificial neural networks (ANN) uses artificial neurons to process information. It is used to evaluate complex nonlinear problems with sizable data sets. It also analyzes problematic data sets that are difficult to tackle ordinarily. Adaptive neuro-fuzzy inference systems (ANFIS) is a kind of artificial intelligence model or concept that utilizes the learnings of fuzzy logic and neural networks to generate a hybrid model that yields an effective and precise result. ANFIS applies to both linear and nonlinear systems with a great level of accuracy. It is also a kind of ANN that is based on a Takagi-Sugeno fuzzy inference system (Gonzalez *et al.* 2020). The objective of this work was to study the effect of acid activation on the adsorptive properties of Ihiala clays on the removal of pollutants from Congo red dyes from an aqueous solution. It also utilizes artificial intelligent optimization models such as RSM, ANN, and (ANFIS) in modeling and predicting the optimum removal of CR dye from wastewater.

2.0. Materials and methods

The primary raw material used is milk-colored clay obtained from Uzoakwa village in Ihiala Local Government Area of Anambra State, Nigeria, while the secondary raw materials used were all of analytical grade and bought from Bridge Head Market in Onitsha, Anambra State. All the solutions used were prepared with distilled water.

2.1 Acid activation of clay sample

The clay material for activation was sun-dried for three days and pulverized using a laboratory mortar and pestle. The mesh clay sample was sieved using 50 µm particle-size dry test sieves. The sieved clay sample was mixed with hydrochloric acid (HCl) in a conical flask in a w/v ratio of 1:6 (200g of meshed clay sample was dissolved with 1200 ml of the prepared acid) and allowed for 24 hours. The slurry was filtered after 24 hours to separate the clay from the acid. The obtained clay residue was washed with distilled water until a neutral pH point was reached with a pH indicator. The neutral clay slurry was dried at an oven temperature of 80 ^{o}C for 240 seconds (4 hours). The obtained dried activated sample was crushed, sieved using 50µm particle-size dry test sieves, and stored in a desiccator until used.

2.2 Characterization

The activated and raw clay samples were analyzed to determine the functional group present and observe surface morphologies. The functional group analysis is also called Fourier transform infrared (FTIR) analysis, and it was carried out using the Shimadzu spectrophotometer model S8400 with samples prepared by the conventional KBr disc method. The surface morphology analysis is also called scanning electron microscope (SEM) analysis, and it was carried out using the Joel scanning electron microscope model JSM 6400 with a coated gold film of layers approximately 20–25 A thick.

2.3 Batch Adsorption Studies

Batch adsorption studies were conducted to investigate the process parametric effects of adsorbent particle size, adsorbent dose, initial adsorbate concentration, adsorption time, pH, and temperature on CR uptake on modified clay adsorbent. A CR solution was prepared by dissolving a known quantity of dye crystals in distilled water. The solution obtained was used as a stock solution and diluted to the required initial concentration range of 100 to 300mg/L. The pH adjustment of the solution was achieved by using either 0.1N HCl or Sodium hydroxide (NaOH). The effect of the studied process variables on CR uptake was determined using a UV-visible spectrophotometer for color removal, a conductivity meter for total dissolved solids (TDS) and electrical conductivity (EC) removal, and a chemical oxygen demand analyzer for chemical oxygen demand (COD) removal.

2.4 Equilibrium/isotherm studies

The equilibrium adsorption experiment was carried out by contacting a fixed quantity of adsorbent into glass beakers (200 ml) containing a definite volume of different concentrations of CR dye solution at the same pH level. These beakers containing the mixture or solution were placed on shakers (magnetic stirrers) regulated at a fixed temperature level for 130 minutes to ensure equilibrium was reached. The equilibrium concentration of the dye is determined using a UV-visible spectrophotometer.

At equilibrium, dye uptake 'qe' (mg g^{-1}), was evaluated using the expression of equation 1

$$qe = \frac{C_f V}{m} \quad (1)$$

Percentage dye uptake was evaluated using equation 2.

$$\% \text{ Adsorption} = \frac{C_f}{C_i} \times 100 \quad (2)$$

Where C_f is the difference between initial and equilibrium dye concentrations (C_i and C_e(mg/L)) were initial and equilibrium dye concentrations respectively, while V and m were the volume of the solution in liter and the mass of dry sorbent used in gram.

The adsorption isotherm is of paramount importance in any adsorption system because it describes the relationship between the adsorbate and adsorbent. In this research work, seven isotherm models were employed: the Langmuir (Langmuir 1916), the Freundlich (Freundlich 1906), the Temkin (Temkin and Pyzhev 1940), the Dubinin-Redushkevich (Dubinin and Redushkevich 1947), the Redlich-Peterson (Redlich-Peterson 1959), and the Jovanovic (Jovanovic 1969), with their expressions (non-linearized forms) listed in equations 3–8. The parameters of each model provide vital information on the adsorption mechanisms, surface properties, and adsorbent affinity.

2.4.1 Langmuir adsorption isotherm

Langmuir's theory postulates that the adsorption process is a surface phenomenon, meaning that it takes place at the adsorbent surface, and equilibrium occurs when the adsorbent site has been sufficiently saturated with dye molecules, which prevents further adsorption from taking place. The saturation point of the adsorbent site is also called the equilibrium adsorption point. The Langmuir adsorption model is a two-parameter model established to define gas-solid-phase adsorption. This empirical model is devised under the presumption that the adsorbed layer has a thickness of one molecule (monolayer adsorption). Additionally, the theory equally presumes that adsorption is constrained to a small number of indistinguishable sites and that no lateral relationship exists between the molecules adsorbed on closed neighboring sites. Langmuir isotherm expression describes adsorption homogeneity (homogeneous adsorption) as a process where all active sites have even energies and indistinguishable affinity for adsorbate onto the surface without the migration of molecules between localized surfaces. The non-linearized form of the Langmuir model can be expressed as follows:

$$q_e = \frac{q_{max} K_L C_e}{1 + K_L C_e} \qquad (3a)$$

Where q_{max} (mg/g) is Langmuir adsorption capacity constants, K_L (L/mg) is Langmuir energy/affinity of adsorption constants, C_e (mg/L) is the equilibrium concentration, and q_e (mg/g) is the amount of dye adsorbed at equilibrium.

When the K_L value is high (greater than 1), it indicates that the adsorbate molecules have a high affinity for the adsorbent surface (strong adsorption). A K_L value of unity (K_L = 1) implies that the adsorption process is at equilibrium, with no significant preference for adsorption or desorption. When K_L is greater than zero but less than unity (0 < KL < 1), it indicates that the gas molecules have a low affinity for the adsorbent (weak adsorption). Finally, a K_L value of zero (K_L = 0) implies that there is no interaction between the adsorbate and the adsorbent (no adsorption).

The essential feature of the Langmuir isotherm was expressed using R_L, a dimensionless constant referred to as the separation factor or equilibrium parameter. R_L is calculated using the expression of equation 3b.

$$R_L = \frac{1}{1 + K_L C_o} \qquad (3b)$$

The value of R_L classifies the adsorption process into the following categories: unfavorable (R_L >1), linear (R_L =1), favorable (0<R_L<1), or irreversible (R_L=0).

2.4.2 Freundlich adsorption isotherm

The Freundlich model presumes that the adsorption process occurs on heterogeneous solid surfaces (non-uniform surfaces with a varying range of adsorption energies). The Freundlich adsorption isotherm is a two-parameter isotherm that explains the relationship between the pressure or concentration of the adsorbate at a constant temperature and the quantity of adsorbate adsorbed onto an adsorbent (a solid surface). The non-linearized form of the Freundlich model can be expressed as follows:

$$q_e = K_F C_e^{\ 1/n_F} \qquad (4)$$

Where C_e (mg/L) is the equilibrium concentration, q_e (mg g^{-1}) is the amount of dye adsorbed at equilibrium, K_F is Freundlich adsorption capacity and affinity constants, and n is the Freundlich adsorption intensity and mechanism constants, $1/n_f$ is a measure of the surface heterogeneity of the adsorption site.

When the n value is close to unity (1), it signifies that the adsorption sites have uniform energies, thereby suggesting a more homogeneous solid surface. This outcome certifies that the adsorption process will be better suited to BET or Langmuir isotherms. When the n value is "n < 1 or n > 1," it indicates that adsorption sites have non-uniform energies, which makes the surface more heterogeneous. This outcome certifies that the adsorption process will be best described by the Freundlich isotherm model, which is better suited to heterogeneous surfaces (adsorbents with varying adsorption energies across the surface). The n_f value within the range of 1<n_f<10 indicates favorable and physical adsorption, whereas any value outside the range of 1<n_f<10 suggests a linear and chemical process. When the K_F value is high, it indicates a greater affinity of the adsorbate for the adsorbent, which leads to a higher adsorption

capacity of the adsorbent, whereas a smaller value of K_F suggests a weaker affinity of the adsorbate for the adsorbent, resulting in poor adsorption capacity.

2.4.3 Temkin adsorption isotherm

The Temkin adsorption isotherm presumes that the heat of adsorption is constant and decreases linearly with coverage as a result of adsorbate-adsorbent interaction on the surface. Therefore, the Temkin adsorption isotherm is a mathematical model used to describe the heat of adsorption and the adsorbate-adsorbent interaction on a surface, or it's a thermodynamic model used to describe the adsorption of gas molecules onto a solid surface. This model is an extension of the Freundlich and Langmuir isotherm models, but it places more emphasis on predicting adsorption behavior in heterogeneous systems where the adsorption sites and energy are not uniform. This model is more suited to real-world processes compared to the Langmuir model, which assumes a uniform energy distribution of adsorption sites and monolayer adsorption. The non-linearized form of the Temkin model can be expressed as follows:

$$q_e = \frac{RT}{a_T} \ln(A_T C_e) \tag{5}$$

Where a_T is the Temkin constant related to the heat of adsorption and the coverage of the surface, A_T (l/g) is the equilibrium binding constant related to the maximum binding energy, R is the universal gas constant (8.314 J/mol K), T is the temperature in Kelvin, C_e (mg/L) is the equilibrium concentration, q_e (mg g^{-1}) is the amount of dye adsorbed at equilibrium.

When the value of a_T is high, it indicates a greater decrease in adsorption energy with increasing surface coverage, which means stronger interactions between the adsorbate and the adsorbent. A higher value of A_T indicates a broader distribution of adsorption energies, suggesting that the adsorption process involves various energy levels.

2.4.4 Dubinin-Radushkevich (D-R) adsorption isotherm

The Dubinin-Radushkevich isotherm model postulates that adsorption occurs due to the formation of indistinguishable energy wells within the porous structure of the adsorbent. These wells are formed by the interactions between the adsorbate molecules and the adsorbent. Additionally, this empirical model is used to represent the adsorption mechanism on surfaces with variability in adsorption energies using a Gaussian distribution of photon energy. The D-R isotherm also estimates the maximum adsorption capacity (q_{max}) of the adsorbent, which is an important parameter for evaluating the performance of an adsorbent. The non-linearized form of the Dubinin-Radushkevich model can be expressed as follows:

$$q_e = q_{max} \exp\left(-b_{DR}\left[RT\, ln\left(1 + \frac{1}{C_e}\right)\right]^2\right) \tag{6}$$

Where q_{max} (mg/g) is the maximum adsorption capacity constant, C_e (mg/L) is the equilibrium concentration, and q_e (mg g^{-1}) is the amount of dye adsorbed at equilibrium. b_{DR} is a constant related to the adsorbent's structural characteristics and the energy distribution of the adsorption sites.

The adsorption mechanism is being examined through the mean free energy "E" value obtained from the D-R model. The D-R model constant b_{DR} relates to the mean free energy of adsorption through the expression of equation 6b.

$$E = \frac{1}{\sqrt{2b_{DR}}} \tag{6b}$$

When the b_{DR} value is small, it suggests a narrow energy distribution and probably a possible homogeneous system, whereas a larger value of b_{DR} indicates a broader energy distribution and a possible heterogeneous system.

A high value of k_{vs} signifies that the adsorbent has a strong affinity for the gas molecule, whereas a low value indicates weak interaction. A high value of B_{vs} suggests strong interaction between adsorbed molecules, whereas a low value indicates poor interaction.

2.4.5 Redlich–Peterson (R-P) isotherm

The Redlich-Peterson isotherm model is a three-parameter isotherm. The model design equation incorporates the feature of Freundlich and Langmuir, which signifies that it describes the adsorption on both heterogeneous and

homogeneous surfaces. Redlich-Peterson invents this empirical equation to shed more light on the adsorption behavior of real systems, which deviate from the simplified presumptions made individually by the Freundlich and Langmuir isotherms.

The non-linearized form of the R–P model can be expressed as follows:

$$q_e = \frac{K_R C_e}{1 + a_R {C_e}^g} \quad (8)$$

Where C_e (mg/L) is the equilibrium concentration, q_e (mg g^{-1}) is the amount of dye adsorbed at equilibrium, K_R (L/g) is constant related to the adsorption capacity and affinity of the adsorbent, a_R (L mg^{-1}) is constant related to the adsorption capacity, and g (dimensionless) are the Redlich–Paterson constant. The values of g fluctuate between 0 and 1. A low g value (g tends to zero) suggests heterogeneous adsorption characteristics of Freundlich isotherm (Henry's law), while a high g value very close to unity signifies homogeneous or monolayer adsorption characteristics of Langmuir isotherm. Additionally, the g value helps to interpret the extent to which a gas digresses from ideal gas behavior, with higher values suggesting closer adherence to ideal gas behavior and lower values suggesting more significant deviations due to stronger intermolecular forces.

When the a_R value is high, it indicates the adsorbent has a good ability to adsorb and retain more adsorbate molecules at a given temperature, whereas a low value signifies poor adsorption and retaining ability of the adsorbent. When the K_R value is high, it indicates the adsorbent has a great adsorption capacity and affinity for the adsorbate, whereas a low value signifies poor adsorbent adsorption capacity and affinity for the adsorbate.

2.4.6 Jovanovic adsorption isotherm

The Jovanovic isotherm model is a two-parameter isotherm designed based on the assumptions of the Langmuir isotherm model but assumes surface adsorption and zero correlation between molecules. This empirical model permits some mechanical contact between the adsorbent and the adsorbate and accepts the surface vibration of an adsorbed species. It can also be used for adsorption with both mobile and confined monolayers without lateral contact, however, it is less effective in physical adsorption due to the adjustment of the adsorption surface from this model. Furthermore, the Jovanovic isotherm model equation simplifies Freundlich isotherm (Henry's law) at low concentrations and can reach the saturation limit at high concentrations. The non-linearized form of the Jovanovic model can be expressed as follows:

$$q_e = Q_m(1 - exp^{-K_J C_e}) \quad (9)$$

Where q_m (mg/g) is Jovanovic adsorption capacity constants, C_e (mg/L) is the equilibrium concentration, and q_e (mg g^{-1}) is the amount of dye adsorbed at equilibrium. K_J (L mg^{-1}) is the equilibrium constant of Jovanovic isotherm and it represents the adsorption affinity of the adsorbate for the adsorbent. It also helps to determine the extent of adsorption at different concentrations.

2.5 Kinetic Studies

In kinetic experiments, aqueous samples were taken at different time intervals to determine the uptake of dye at any preset time t.

At time t, dye uptake 'qt' (mg g^{-1}) was evaluated using equation 10

$$qt = \frac{(C_i - C_t)V}{m} \quad (10)$$

Where C_t is dye concentration at any time t.

Adsorption kinetics is a very vital aspect of the adsorption system, which sheds light on the mechanism of adsorption and the adsorption dynamics with time. In this research work, nine kinetic models were employed: the pseudo-first-order (Lagergren 1898), the pseudo-second- order (Ho *et al.* 1996, Ho and Makay 1999), the Elovich (Elovich and Larionov 1962), the pseudo-nth-order model (Ritchie 1977), the Avrami (Avrami 1939) the Fractional Power (Dalal 1974), intra-particle diffusion (Weber and Morris 1963), the Bangham pore diffusion (Aharoni and Ungarish 1977),

the liquid film (Spahn and Schlunder 1975), and the Boyd models (Boyd *et al.* 1947). The liquid film, Bangham pore diffusion, intra-particle diffusion, and Boyd model were proposed to identify the adsorption mechanism.

2.5.1 Pseudo-first-order (PFO) model

The pseudo-first-order kinetic postulates that the rate of the reaction appears to depend on the concentration of one reactant, but in reality, it may involve other factors as well. The pseudo-first-order kinetic model is an empirical method used to analyze the rate of a chemical reaction or other process. The model is called "pseudo" because it may not precisely replicate a true first-order reaction, but rather, it is a simplified approach used to estimate the reaction kinetics. Additionally, this model is very useful when one of the reactants is present in excess and its concentration does not significantly change during the reaction; therefore, the model is suitable for analyzing reaction kinetics and understanding the factors affecting the reaction rate. The non-linearized form of the pseudo-first-order model can be expressed as follows:

$$q_t = q_e[1 - exp(K_1 t)] \tag{11}$$

Where q_e (mg/g) is the amount of adsorbate adsorbed at equilibrium, q_t (mg/g) is the amount of adsorbate adsorbed at time t. K_1 (min^{-1}) is the adsorption rate constant for pseudo-first-order.

2.5.2 Pseudo-second-order (PSO) model

The pseudo-second-order kinetic theory postulates that the concentration of the adsorbate and the product of the remaining accessible adsorption sites determine the rate of reaction, so the kinetic model is an empirical model used to analyze the reaction kinetics of different chemical processes. The pseudo-second-order model is an extension of the conventional second-order kinetic model, and it gives more detailed knowledge to chemical systems where the reaction rate depends on the surface coverage of adsorbed species. This kinetic model also provides a more detailed image of overall kinetics than the first-order model, especially when the adsorption process is multi-step. Furthermore, the pseudo-second-order model aids in determining the rate-determining step of the adsorption process. The non-linearized form of the pseudo-first-order model can be expressed as follows:

$$q_t = \frac{K_2 q_e^2 t}{1 + K_2 q_e t} \tag{12}$$

Where q_e (mg/g) is the amount of adsorbate adsorbed at equilibrium, q_t (mg/g) is the amount of adsorbate adsorbed at time t, K_2 $gmg^{-1}min$ were the adsorption rate constants pseudo-second-order.

2.5.3 Elovich model

The Elovich kinetic theory postulates that the adsorbent surfaces are energetically heterogeneous. This model presumes that the adsorption kinetics will not be affected by interactions between the adsorbed and desorption ions, even at low surface coverage. The major effect of energetic heterogeneity surfaces on sorption equilibrium in gas-solid systems has been proven, while that of liquid-solid systems is yet to be established. The non-linearized form of the pseudo-first-order model can be expressed as follows:

$$q_t = \frac{1}{B}\ln(1 + ABt) \tag{13}$$

Where q_t (mg/g) is the amount of adsorbate adsorbed at time t, A is the Elovich constant for the initial adsorption rate, and B is the Elovich desorption constant.

When the value of A is high, it suggests a faster initial adsorption rate, meaning that the adsorbent has a high affinity for the gas molecule, whereas a smaller value of A indicates a slow initial adsorption rate. A higher value of B suggests high adsorption capacity, which means that the adsorbent surface cannot easily desorb the adsorbate molecules, whereas a small value of B indicates poor adsorption capacity.

2.5.4 Pseudo-nth Order (PNO)

The pseudo-nth-order kinetic model is an empirical model used to analyze chemical systems where the reaction order is not naturally an integer, and it's an extension of the first- and second-order kinetic models. The model can be applied to different types of reactions, which include heterogeneous and homogeneous reactions. Additionally, the pseudo-nth-order kinetic model can also be applied to reactions where the order of reaction cannot be easily determined, and

it can also analyze and predict the behavior of different reactions, which include mass transport processes, all catalyzed reactions, and electrochemical reactions. The non-linearized form of the pseudo-first-order model can be expressed as follows:

$$q_t = q_e - [q_e^{1-n} - (1-n)K_n t]^{1/(1-n)} \quad (14)$$

Where q_e (mg/g) is the amount of adsorbate adsorbed at equilibrium, q_t (mg/g) is the amount of adsorbate adsorbed at time t. K_n ($gmg^{-1}min$) were the adsorption rate constants for pseudo-nth-order; n is the order of the reaction.

When the value of n is high (n > 1), it indicates that the rate of reaction of the reactant concentration is likely to change, whereas a smaller value of n (0 < n < 1) suggests that the reaction rate of the reactant concentration is unlikely to change. A value of n = 1 represents a first-order reaction, while n = 0 represents a zero-order reaction. A high k value suggests a faster reaction rate, whereas a smaller value indicates a slower reaction rate. The rate constant can be used to calculate the half-life of the reaction or the time required for the reaction progress variable (x) to reach a specific value.

2.5.5 Avrami model

The Avrami kinetic model presumes that the adsorbent surface possesses random nucleation sites across the reaction surface. This model evaluates changes in kinetic parameters as a function of temperature and reaction time. The Avrami kinetic model was initially developed by Kolmogorov et al. (1937) and made popular by Avrami (1939). The non-linearized form of the Avrami model can be expressed as follows:

$$q_t = q_e\{1 - \exp[-(K_{AV}t^{n_{AV}})]\}$$

Where q_e (mg/g) is the amount of adsorbate adsorbed at equilibrium, q_t (mg/g) is the amount of adsorbate adsorbed at time t, K_{AV} is the Avrami constant, which depends on the reaction mechanism and the system's properties. It is dimensionless and typically ranges between 0 and 1, which n_{AV} is the Avrami exponent, which depends on the spatial dimension and the geometry of the growing phase. It can be a fraction or an integer, and its value determines the shape of the reaction progress curve, and t is time which is the independent variable in this equation.

2.5.6 Fractional power (FP) model

The fractional power kinetic model is a modified form of the Freundlich model. This empirical model calculates the exact rate of adsorption at a unit time using the model product's constant. The non-linearized form of the pseudo-first-order model can be expressed as follows:

$$q_t = Kt^V \quad (15)$$

Where q_t (mg/g) is the amount of adsorbate adsorbed at time t, this parameter "t" should not contain a value equal to zero to prevent infinite value. K(mg g-1) is the fractional power constant and v is the fractional power rate constant.

2.6 Adsorption Thermodynamics

Thermodynamics studies were to determine the energy changes involved in the adsorption. Thermodynamic parameters are calculated using the following equations

$$\Delta G^0 = \Delta H^0 - T\Delta S^0 \quad (16)$$

$$\Delta G^o = -RT \ln K_c \quad (17)$$

Where $K_c = \frac{C_S}{C_e}$ (17a)

$$\ln K_c = \left(\frac{\Delta S}{R}\right) - \left(\frac{\Delta H}{RT}\right) \quad (18)$$

Where ΔG^o, ΔH, ΔS are the standard; Gibbs free energy change, enthalpy change (heat of reaction) and entropy change, respectively. $K_c$is the equilibrium constant, C_s is the equilibrium concentration of CR on solid (adsorbent (mg/L)), R is the general gas constant (8.314J/mol/K) and T is adsorption temperature on the Kelvin scale.

2.6.1 Activation energy

The nature of the adsorption process can be inferred from the level of activation energy. The Arrhenius rate expression of equations (19) and (20) was used to evaluate the activation energy of adsorption.

$$K_A = Ae^{-Ea/RT} \tag{19}$$

$$InK_A = InA - \frac{Ea}{RT} \tag{20}$$

Where Ea is the Arrhenius activation energy (KJ/mol) K_A is a pseudo-second-order rate constant of adsorption (g/mg min), R is the universal gas constant (8.314J/molK) and T is the absolute solution temperature (k). Ea Can be calculated from the plot of InK_A versus 1/T.

2.7 RSM modeling

Design expert version 13 was used in both the design and the RSM-CCD analysis. The experiment was designed using a central composite design (CCD) with five-factor levels as shown below in Table 1. RSM uses data obtained from the design of experiments and statistical modeling techniques to solve multi-variant problems (Venkatesh and Karthikeyan 2018).

Table 1: Five-factor levels of the independent variables

Process parameter	**+α**	**+1**	**0**	**-1**	**-α**
Temperature (°C)	54.1421	50.00	40.00	30.00	35.8579
Concentration (mg/l)	582.843	500.00	300.00	100.00	17.1573
pH	12.864	11.00	6.5	2	0.1360
Particle size (μm)	994.975	850	500	150	5.02525

The independent variables used were temperature, pH, concentration, and particle size while the actual response (percentage adsorbed) was the dependent variable. The number of data sets for the RSM-CCD experiment can be evaluated using the expression of equation (21) (Arulkumar *et al.* 2011).

$$Q = 2^q + 2q + q_c \tag{21}$$

Where q is the number of input factors and 2^q, 2q and q_c represents the: factorial points, axial points, and center points. Furthermore, the total number of factorial and star points was tripled to maximize the dependability of the design and ten center points were used. As a result, a total of 82 experimental data sets were assessed. The experiment was conducted at random to eliminate systematic error. The link between the process variables and dependent variables was estimated using the second-order polynomial as in equation (22).

$$R = \beta_o + \sum_{i=1}^{k} \beta_i \alpha_i \ldots\ldots + \ldots \sum_{i=1}^{k} \beta_{ii} \alpha_i^2 \ldots\ldots + \cdots \sum_{i=1}^{k-1} \sum_{j=1}^{k} \beta_{ij} \alpha_i \alpha_j \tag{22}$$

Where R is the calculated response, β_o is the model constant, β_i, β_{ii} and β_{ij} are the calculated coefficients second-order polynomial expression for the linear, quadratic and products of α_i, α_i^2 and $\alpha_i \alpha_j$, respectively.

2.8 ANN modeling

Artificial neural networks (ANN) were used to model and analyze the percentage of CR dye adsorbed using the neural network toolbox of MATLAB R2021. The weighted inputs that arrive at each neuron in a biological system are processed through a nonlinear activation function to create an output signal (Manpreet *et al.* 2011). The data sets used in RSM-CCD analysis were tripled and used in the ANN for an accurate modeling process. The validation, training, and testing data sets each received a randomly assigned percentage of 15%, 70%, and 15% of the total data sets. The ANN architecture comprises the input nodes, hidden neuron layers, and output nodes. See Figure1.

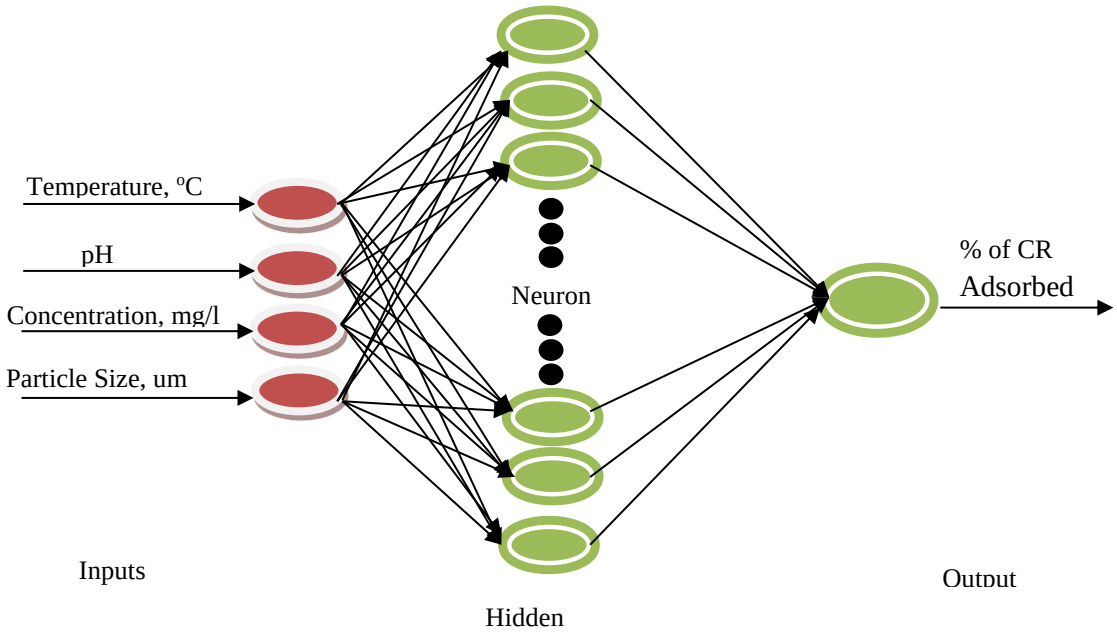

Figure 1: ANN architecture of CR removal

To prevent over-fitting and a decrease in the convergence rate, the optimal number of hidden layers was established by iteration (Mingyi *et al.* 2017). The metrics were maximum correlation coefficient (R^2) and minimum mean square error (MSE). The learning approach for the modeling was a Multi-Layer Perceptron (MPL) that used backpropagation. The training function, trainlm, was utilized to regularize the bias value. To lessen network error, the process parameters and the response were standardized between 0 and 1 (Mourabet *et al.* 2014).

2.11 ANFIS modeling

ANFIS model was used to model and predict the optimum CR dye adsorbed, through Mathworks Inc. R2021. The ANFIS is represented as a five-layered network using the fuzzy inference system (FIS) concept, as shown in Figure 2. Temperature, concentration, particle size, and pH are the process variables that the first layer of the fuzzy system network accepts as inputs. The fuzzy rules were chosen in the second layer node and passed on to the third layer so that the activity rules could be normalized.

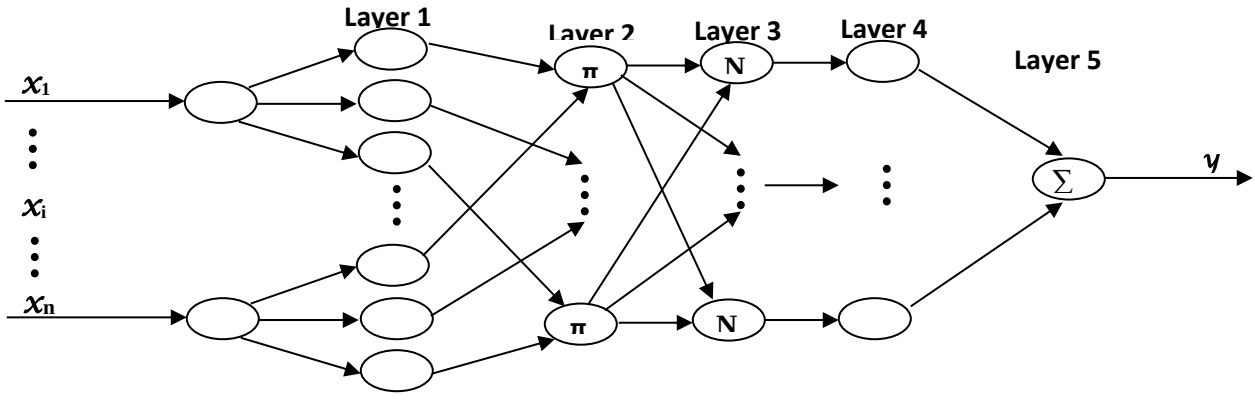

Figure 2: ANFIS structure

The fourth layer accepts the nodes, converges the parameters, and sends them as a single output layer (percentage of CR adsorbed) to the fifth layer (Bahman *et al.* 2018). The ANFIS modeling utilized the same set of data as the ANN modeling (two hundred and forty-six data sets). A hybrid optimization approach was applied with zero error tolerance.

2.12 Comparative analysis of RSM, ANN, and ANFIS models

The actual CR adsorption values were compared to the predicted adsorption values by RSM, ANN, and ANFIS and subjected to statistical error indices. Five out of the seven statistical error functions given in Table 2 were used for comparative analysis. The normalized standard deviation, Chi-square test, average percentage error, and root mean square error functions were statistical error tools used to determine the best-fit equilibrium and kinetic model for the system.

Table 2. Statistical error functions used

Error function	Equation	Eqn. Num.
Correlation coefficient	$R^2 = 1 - \frac{\sum_{i=1}^{N}(\mathrm{M_{exp}} - \mathrm{M_{pre}})^2}{\sum_{i=1}^{N}(\mathrm{M_{exp}} - M_m)^2}$	(23)
Average relative error	$ARE = \sum_{i-1}^{N} \frac{\left\lvert q_{e\,exp} - q_{e\,cal}/q_{e\,exp}\right\rvert}{N} X\ 100$	(24)
Sum of the squared error	$\mathrm{SSE} = \sum_{\mathrm{i=1}}^{\mathrm{N}} \left(\mathrm{M_{exp}} - \mathrm{M_{pre}}\right)^2$	(25)
Root mean square error	$RMSE = \sqrt{\frac{1}{N-2}\sum_{i=1}^{N}\left(\mathrm{M_{exp}} - \mathrm{M_{pre}}\right)^2}$	(26)
Hybrid fractional error function	$HYBRD = \frac{100}{n-p}\sum_{\mathrm{i=1}}^{\mathrm{N}} \frac{\left(\mathrm{M_{exp}} - \mathrm{M_{pre}}\right)^2}{\mathrm{M_{exp}}}$	(27)
Normalized standard deviation	$NSD = 100 \times \sqrt{\frac{\sum_i^N [(q_e \exp - q_e cal)/q_e exp]^2}{N-1}}$	(28)
Chi-square test	$x^2 = \sum_{N=1}^{N} \frac{(q_{e,exp} - q_{e,cal})^2}{q_{e,cal}}$	(29)
Sum of absolute error	$\mathrm{EABE} = \sum_{\mathrm{i=1}}^{\mathrm{N}} (qe_{exp} - qe_{cal})$	(30)
Mean square error	$\mathrm{MSE} = \frac{1}{n-2}\sum_{\mathrm{i=1}}^{\mathrm{N}} \left(qe_{\mathrm{exp}} - \mathrm{qe_{cal}}\right)^2$	(31)

Where N is the number of experimental runs; $\mathrm{M_{exp}}$ is the experimental values for the modeling; $\mathrm{M_{pre}}$ is the model predicted value; $M_m$is the experimental mean value, $q_{e,exp}$ and $q_{e,cal}$ are the experimental values and model calculated values respectively.

These error functions were used to investigate the accuracy of the models in predicting the removal of CR from aqueous solutions by the adsorption process. The significance of the sum of squared errors (SSE), average percentage error (APE), Hybrid fractional error function (HYBRID), Root mean square error (RMSE), mean square error (MSE), and sum of absolute error (EABE) models was based on the fact that the smaller the values of the result, the better the system, while the correlation coefficient (R^2) is that the higher the value of the result to unity, the better the system.

2.13 Dissolve Salts and Solid Analysis

This analysis was carried out using a DDS-307A conductivity meter. The conductivity meter displays both electrical conductivity (EC) and total dissolution solids (TDS) results. This meter possesses a temperature sensor and a conductivity probe. The probe is labeled with a cell constant. Before every measurement, the probe tip was rinsed with distilled water and the sample, and after immersing the conductivity probe into the sample for a measurement, the sample was stirred with a glass bar to achieve an ideal condition for an accurate answer.

2.13 Chemical Oxygen Demand (COD) Analysis

This analysis was carried out using Lovibond water testing RD 125 and Lovibond water testing Photometer-System MD 200. The RD 125 is the reactor used to digest the vials after mixing each with 2 ml of the samples and one with distilled water used as a blank for 120 minutes at a temperature of 150 °C or less.

2.10 Adsorbent Recycling and Regeneration

Recycling is the process of processing materials that would have otherwise been thrown away as trash into new products, which minimizes production costs as well. This phenomenon in the adsorption process is termed desorption. Desorption is simply using an eluent to create sorption equilibrium or destabilize the bond between the pollutant (bulk phase) and the adsorbing surface. Different desorption methods, including chemical regeneration, thermal regeneration, thermochemical regeneration, steam regeneration, bio-regeneration, vacuum regeneration, electrochemical regeneration, pressure swing regeneration, ozone regeneration, microwave regeneration, oxidative regeneration, and ultrasound regeneration, have been used in the regeneration or recycling of adsorbents. In this research, a chemical regeneration method was employed, and the eluents used were acid and base.

2.10.1 Batch desorption.

The exhausted adsorbent was mixed with the eluent and stirred at a specific temperature for 30 minutes per cycle until equilibrium was reached. It was then filtered into filtrate and residue adsorbent at the end of each cycle. The filtrate was for dye analysis using a UV spectrophotometer for desorption efficacy, while the residue sorbent was washed with water to remove the eluting agent, which was then oven-dried and kept for reuse in a fresh process. The amount (quantity) in mg/g and efficacy in % of desorbed adsorbate (pollutant) were calculated using equations (32) and (33), respectively.

$$\text{Amount /quantity desorbed (mg/g)} = A_{des} = \frac{C_s * V}{M} \quad (32)$$

$$\text{Efficiency of desorbed (\%)} = \%_{des} = \frac{A_{des}}{C_{ad}} X\ 100 \quad (33)$$

Where, C_s is the concentration of adsorbate desorbed in mg/g, C_{ad} is the concentration of adsorbate adsorbed in mg/g, M is the weight of exhausted adsorbent in grams and V is the volume of the eluent in liter.

3.0 Results and Discussion

3.1 Characterization Result

3.1.1 FTIR analysis

Fig. 3a, b, and c present the FTIR spectra of raw IHIALA clay (RUC), acid-modified (HCl) Ihiala clay (HIC) and CR adsorbed on HIC. From the spectra of Fig.3a, a higher number of peaks was observed than in Fig.3b which may be a result of acid modification that removes impurities contained in the raw clay material, and the peaks of Fig.3b composed of various functional groups which are responsible for the binding of CR dye e.g. Amide, alkane, alcohol, alkyne halide. Fig.3c also showed spectra of higher peaks than Fig.3b as well which indicates the possible involvement of some functional groups on the surface of the HIC in the adsorption process.

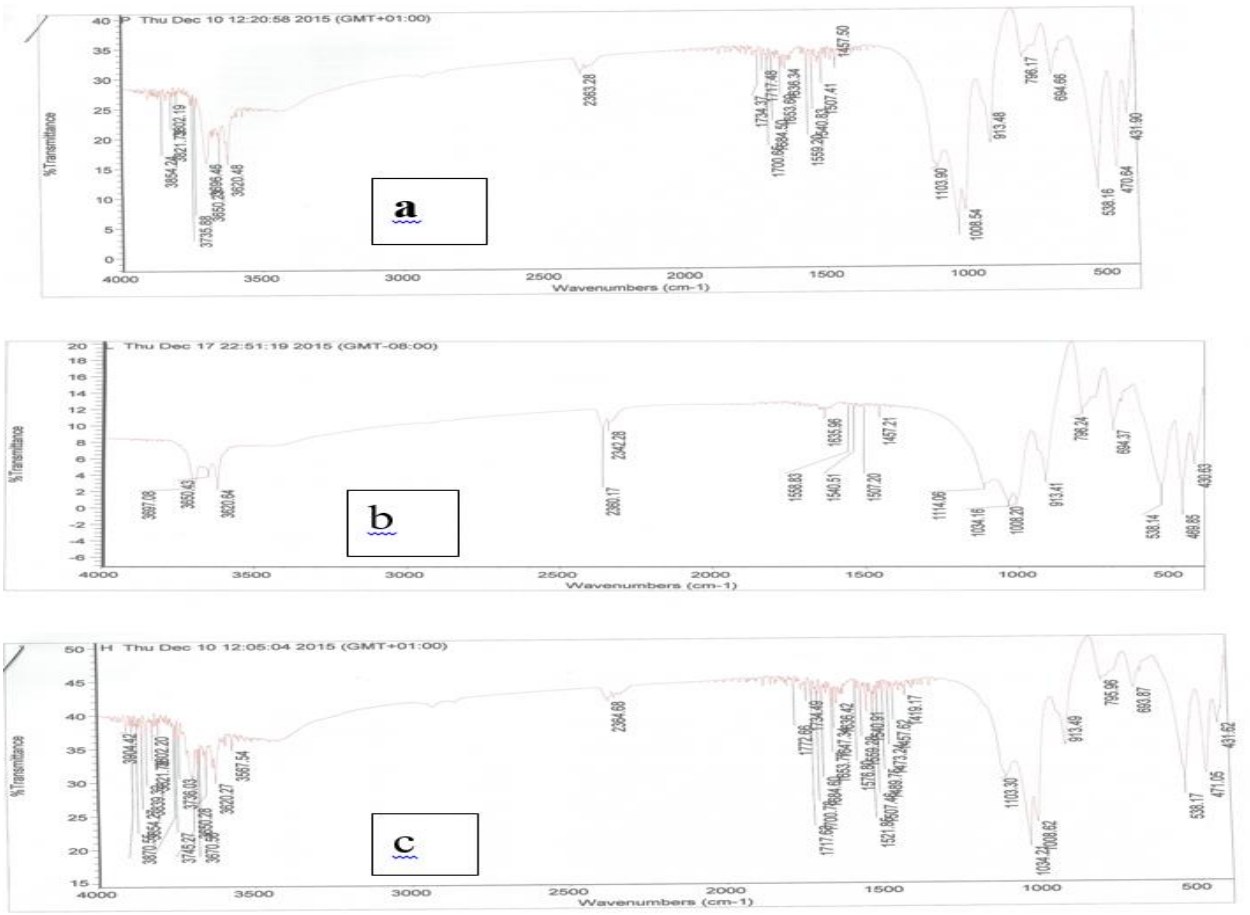

Figure 3: FTIR spectra (a) raw clay, (b) activated clay, (c) after adsorbed clay

3.1.2 SEM micrographs

Fig. 4a, b, and c present the scanning electron micrograph (SEM) of Ihiala clay samples in raw state, activated state, and after CR adsorption on HIC state. Fig. 4b displayed a considerable number of heterogeneous layers of pores and internal surface of the clay material than Fig. 4a, this observed development is a result of modification which exposed the internal surface of the clay sample. Fig. 4c showed a smoother surface which signified adsorption had taken place. The observed smooth surface is dye particles that cover most porous surfaces of Fig. 4b.

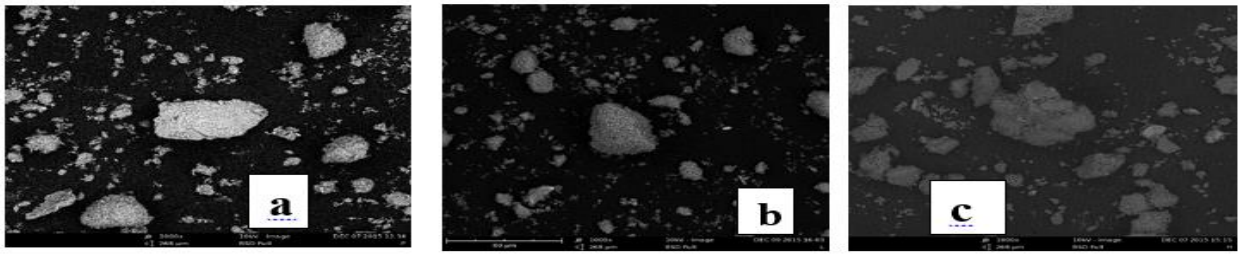

Figure 4. SEM Micrograph of (a) raw clay, (b) activated clay, (c) after adsorbed clay

3.3: Effect of Adsorbent Dosage

The adsorbent dosage effect was investigated for the dosage range of 0.2, 0.4, 0.6, 0.8, and 1g at a constant temperature of 313 k, an adsorbent particle size of 150 µm, a pH of 2, an initial dye concentration of 100 mg/l, and a time of 60

min. The result of the study, as reported in the histogram of Fig. 5a, shows that the percentage of adsorption increases with an increase in adsorbent dosage, from 53.1% at 0.2g to 97.6% at 1g. The observed increase in the percentage adsorption of dyes per increase in adsorbent dosage as a result of the increased surface area of active functional groups, which also gives rise to a greater availability of adsorption sites (Oguanobi *et al.* 2019, Ladhe *et al.* 2011). Moreover, as the adsorbent dosage increased, a significant decrease in the amount adsorbed per unit mass of the adsorbent was observed. This decrease in unit adsorption as adsorbent dosage increases is a result of adsorption sites remaining unsaturated during the adsorption process. The result of this research concurs with the previous reports by Ismat *et al.* (2023) and Oguanobi *et al.* (2019), who reported that an increase in HAC dosage drastically decreased the amount of crystal violet dye in the aqueous solution.

3.4: Effect of Particle Size

The effect of particle size was studied with particle sizes ranging from 75, 150, 300, 600, and 850 µm at a constant temperature of 333 k, an adsorbent dosage of 1 g, an initial dye concentration of 100 mg/l, a time of 60 min, and a pH of 2. The result of the study, as reported in the histogram of Fig. 5b, shows that the percentage of dye adsorption increases with sorbent size, from 60.4% at 850 µm to 98.1% at 75 µm. This is because smaller particles possess a larger surface area and pores than bigger particle sizes. Additionally, the breaking of larger particles opens tiny cracks and channels on the particle surface of the material, resulting in more accessibility and easy diffusion due to the smaller particle size. The outcome of this study concurs with the previous report by Oguanobi *et al.* (2019), who confirmed that an increase in adsorbent particle size distinctly decreased the percentage of dye removed. El-Halwany (2010) and Wu *et al.* (2012) also reported that dye removal increased with a decrease in particle size.

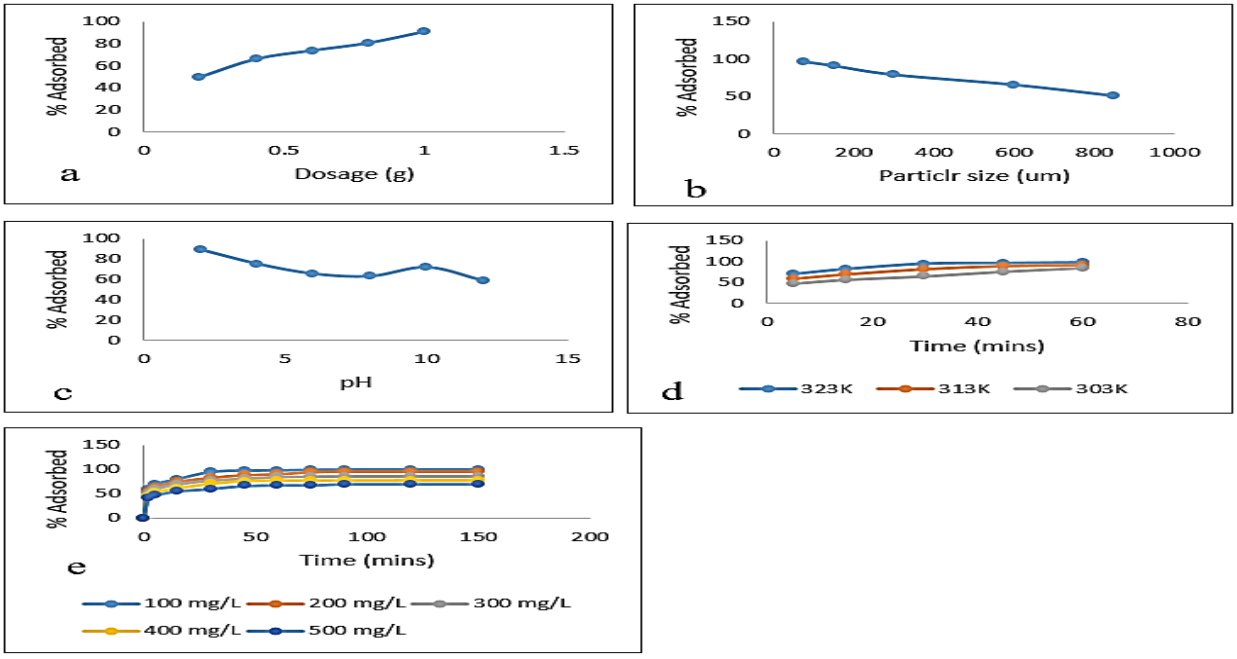

Figure 5: Effects of process parameters displaying the impact of (a) particle size, (b) dosage, (c) concentration, (d) pH, and (e) temperature on the percentage of CR adsorbed

3.5 Effect of pH

The effect of pH is paramount when the adsorbing molecules are capable of ionizing in response to pH. CR is a diazo/anionic dye and maintains its red color at pH 5, while below pH 2, the solution changes from red to dark blue; at pH 3, it changes to blue-violet; and the original red color is different above pH 10. The pH effect is studied between the pH ranges of 2 and 12, at a constant temperature of 323 k, an adsorbent particle size of 75 µm, an initial dye concentration of 100 mg/l, a time of 60 min, and an adsorbent dosage of 1g. The result of the study, as reported in the histogram of Fig. 5c, shows that the highest removal efficiency of 98% was achieved at pH 2, 80.5% at pH 10, and 73% at pH 12. These outcomes are due to the very low solubility of CR at pH < 2. Low pH leads to an increase in H^+ ion concentration in the system, and the surface of the clay acquires a positive charge by adsorbing H^+ ions. As the clay surface is positively charged at a low pH, a significantly strong electrostatic attraction appears between the

positively charged sites and the anionic dye molecules. A negatively charged surface site on the clay does not favor the adsorption of anionic CR molecules due to electrostatic repulsion. The findings of this study concur with previous reports by Imessaoudene *et al.* (2023), Adebayo *et al.* (2022), and Reddy *et al.* (2011), who found that pH 2 was optimal for removing Congo red using CHCFe and Indian Jujube Seeds (IJS) (Zizyphus Mauritania). Popoola *et al.* (2021) and Lafi *et al.* (2019) also reported optimum pH 3 for the removal of Congo red using synthesized coal graphene and activated coffee waste. Moreover, Mahmoud *et al.* (2019) reported that the PNP adsorption on montmorillonite is pH-dependent.

3.6 Effect of Temperature

Temperature as a process variable studies the adsorption thermodynamics and nature, i.e., whether a system is an exothermic or endothermic process. The impact of temperature on CR uptake was examined using a temperature range of 303K, 313K, and 323K at a constant adsorbent dosage of 1g, an adsorbent particle size of 75 µm, an initial dye concentration of 100 mg/l, a pH of 2, and 60 minutes. The result, as reported in the histogram of Fig. 5d, shows an increase in the amount of CR uptake from 91.7% to 99.2% as the temperature of the solution increases. This outcome confirms the adsorption process of CR on HIC as an endothermic system. The observed increase in CR uptake is a result of an increase in the mobility of dye molecules, which may also cause enlargement and disintegration of the internal structure of the adsorbent, thereby enabling large dye molecules to penetrate further. The obtained result is in harmony with the previous report by Oguanobi *et al.* (2019), who reported that CV^+ adsorption on HAC is more energetically favorable to occur at higher temperatures. Mahmoud *et al.* (2019), Mahmoodi *et al.* (2011), and Salleh *et al.* (2011) also reported similar results of the same trend.

3.4 Effect of Concentration and Contact Time

The effect of initial dye concentration was studied at concentration ranges of 100–500 mg L1 per 1 g adsorbent dosage at a contact time range of 60 minutes at a constant temperature of 323 k, an adsorbent particle size of 75 µm, and pH 2. The result, as reported in Fig. 5e, shows that the amount of CR adsorbed per unit mass increased with an increase in initial ion concentration, whereas the adsorption percentage decreased. This outcome is due to the proportion of the initial number of dye molecules to the available surface area at a low concentration. Moreover, an increase in the amount or percentage of adsorption as contact time increases at all initial concentrations until equilibrium is observed. This accounts for the driving force provided by the initial dye concentration to overcome the resistance to the mass transfer of dye between the adsorbate and the adsorbent. Finally, a three-step stage was observed during the adsorption reaction: the bulk diffusion stage (rapid initial adsorption), the pore diffusion and intra-particle diffusion stage (a period of slower uptake), and the equilibrium stage (a period of no significant uptake). The findings of this study are consistent with those of Barakan *et al.* (2019) and Oguanobi *et al.* (2019), who found that at higher ion concentrations of As (V) and CV^+, adsorption efficiency decreased due to a decrease in available active sites. Mahmoud *et al.* (2019) also reported that the equilibrium of the PNP adsorption on the montmorillonite clay was reached after 120 min.

3.7 Equilibrium Modeling

The equilibrium adsorption represents the relationship between the mass of adsorbate adsorbed per unit weight of adsorbent and the liquid-phase equilibrium concentration of the adsorbate (Lata *et al.* 2007). The non-linear expression of Langmuir, Freundlich, Temkin, Dubinin-Radushkevich, Redlich-Peterson, and Jovanovic isotherms were used to analyze equilibrium results. The result in graphical form is reported in Fig. 6. The respective constants of each model were evaluated using software and tabulated in Table 3.

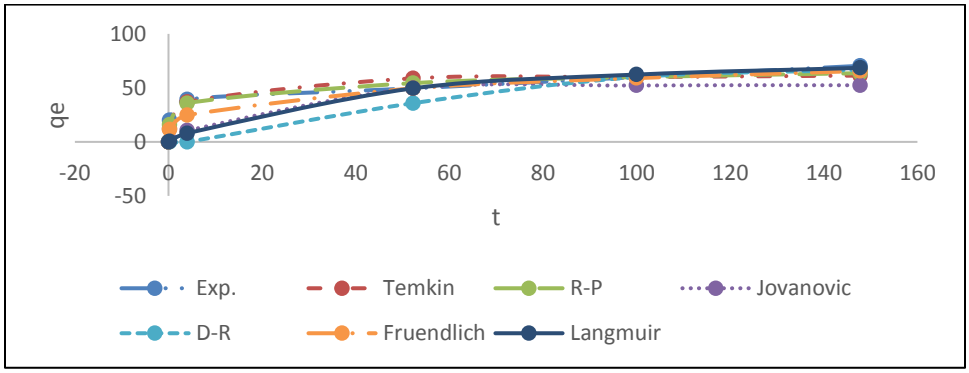

Fig.6. Non-linear isotherm plot for adsorption CR on HIC.

From Table 3, it's seen that Langmuir's maximum adsorption capacity (q_{max}) value is 86.70 The K_L Value of 0.026 indicates that the adsorbate molecules have a high affinity for the adsorbent surface (strong adsorption) and the R_L value of 0.073 as seen in Table 3, certifies favorable uptake of CR dye.

Table 3: Isotherm and Kinetic Parameters for CR Uptake on HIC

Langmuir	**Freundlich**	**Temkin**	**D-R**	**Jovanovic**	**R-P**
q_{max} =86.70	KF=17.06	a_T=313.5	q_{max} =72.9	q_{max} =52.43	Kg=204.8
Kl=0.026	nf =3.709	A_T=18.36	bdr=0.00027	Kj=0.056	a_R =6.702
RL=0.073	1/n= 0.270	-	E=0.043	-	g=0.8528
NSD=5.253	NSD=3.016	NSD=1.067	NSD=8.010	NSD=7.723	NSD=0.989
RMSE=1.328	RMSE=0.558	RMSE=5.239	RMSE=2.161	RMSE=4.491	RMSE=3.954
X^2 =0.052	X^2 =0.335	X^2 = -	X^2 = -	X^2 =4.620	X^2 = -
ARE=4.202	ARE=2.413	ARE=0.853	ARE=6.403	ARE=6.179	ARE=0.791
EABE=50.26	EABE=28.86	EABE=10.21	EABE=76.63	EABE=73.89	EABE=9.457
HYBED=352.0	HYBRD=116.1	HYBRD=14.52	HYBED=818.5	HYBRD=760.9	HYBRD=18.70
MSE=841.9	MSE=277.6	MSE=34.72	MSE=1957.7	MSE=1819.9	MSE=29.81
SSE=2525.7	SSE=832.8	SSE=104.2	SSE=5873.1	SSE= 5459.6	SSE=89.40

PFO	PSO	PNO	Avrami	Fractional	Elovich
ho=2.339	ho=6.383	n=2.161	nav=0.269	V=0.086	B=0.427
K_1 =0.118	K_2 = 0.016	kn=0.032	Kav=0.386	K=12.99	A=172.5
q_e =19.77	q_e =19.81	q_e =19.84	q_e =19.83	-	-
NSD=0.753	NSD=1.333	NSD=0.076	NSD=0.709	NSD=3.848	NSD=1.706
RMSE=0.063	RMSE=0.282	RMSE=0.090	RMSE=0.079	RMSE=0.459	RMSE=0.103
x^2 =1.8x10^{-4}	x^2 =0.034	x^2 =0.008	x^2 =3.1x10^{-8}	x^2 =0.064	x^2=0.003
ARE=0.042	ARE=0.386	ARE=0.198	ARE=0.007	ARE=0.541	ARE= -
EABE=12.17	EABE=10.28	EABE= -	EABE=14.21	EABE=2.724	EABE= -
HYBED=13.26	HYBRD=9.456	HYBRD=4.579	HYBED=21.09	HYBRD=0.665	HYBRD=0.138
MSE=148.9	MSE=15.08	MSE=4.869	MSE=28.83	MSE=1.060	MSE=0.221
SSE=21.16	SSE=105.6	SSE=14.61	SSE=201.8	SSE= 7.422	SSE=1.545

The Freundlich equation is an empirical relationship between the amounts of adsorbate molecules adsorbed onto heterogeneous surfaces. From Table 3, the n_f value of 3.709 indicates that the adsorption sites have uniform energies which indicates the adsorbent surface to be homogeneous. The obtained n_f value confirms the uptake of CR dye as a favorable and physical process. The high n_f value of 3.709 confirms the good affinity of the adsorbate for the adsorbent.

The Temkin model studies the adsorbate-adsorbent interaction on surfaces and the heat of adsorption. From Table 3, a high a_T value of 313.5 indicates a greater decrease in adsorption energy with increasing surface coverage, which means stronger interactions between the adsorbate and the adsorbent, whereas a significant A_T value of 18.36 indicates a broader distribution of adsorption energies, suggesting that the adsorption process involves various energy levels.
The Dubinin-Radushkevich (D-R) isotherm is a temperature-dependent model that forecasts the adsorption mechanism. An adsorption process is physical when the "E" value is below 8 KJ mol^{-1} and chemical, when the "E" value is within the range of 8–16 Kj mol^{-1} (Kausar *et al.* 2013, Singha and Das 2013). From Table 3, the "E" value of 0.043 lies within the range 0-8 KJ mol^{-1} thereby confirming the uptake process of CR dye physical adsorption. The b_{DR} value of 0.00027 in Table 3 is very small, thereby suggesting a narrow energy distribution and probably a possible homogeneous system.

The Redlich-Peterson model embodied both the Freundlich and Langmuir isotherm features. From Table 3, the g value of 0.8528 suggests monolayer adsorption on a homogeneous adsorbent surface. The g value also suggests that the gas deviates more from ideal gas behavior to real gas due to stronger intermolecular forces. This is because the deviation from ideal behavior is more pronounced. The a_R value of 6.702 indicates that the adsorbent has a good ability to adsorb and retain more adsorbate molecules at a given temperature. The K_R value of 204.8 indicates that the adsorbent has a great adsorption capacity and affinity for the adsorbate. The Jovanovic model presumes superficial adsorption and mechanical interaction between the adsorbate and the adsorbent surface. The K_J value of 0.056 indicates good adsorption affinity of the adsorbate for the adsorbent. The high q_{max} values of Langmiur, D-R, and Jovanovic validate the outcome of other parameters likeK_L, $K_{g,}$, n_f, and K_J which confirm the good affinity of the adsorbent for the adsorbate.

3.8 Kinetic Modeling

Adsorption kinetics refers to the study of the rate (how fast or slow) at which an adsorbate (a gas molecule) is adsorbed onto an adsorbent (a solid surface) under specific conditions. For evaluating the adsorption kinetics of CR onto HIC, pseudo-first-order, pseudo-second-order, Elovich, fractional power, Avrami, and pseudo-nth-order kinetic models were used to fit the experimental data. The pseudo-kinetic models assume that adsorption is a pseudo-chemical reaction. When the adsorption processes occur through chemisorption, the Elovich model is most commonly used (Dotto and Pinto 2011). The curve fittings of the models are presented in Fig. 7. The values of the respective constants of the non-linear model were evaluated using Excel software and tabulated in Table 3.

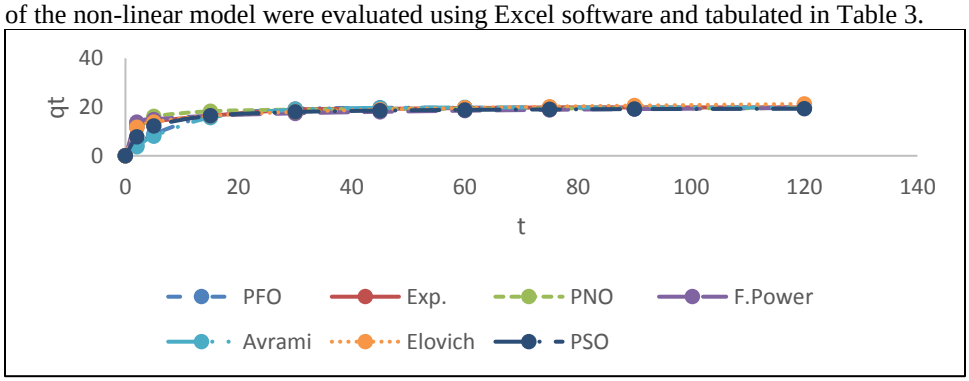

Fig.7: Non-linear kinetic plot for adsorption of CR on HIC. (A plot of q_t against t)

From Table 3, the smaller K_1 value of 0.118 for the pseudo-first-order suggests a slow adsorption process, while the smaller K_2 value of 0.016 for the pseudo-second-order confirms zero correlation with the dye initial concentration, indicating that more than one adsorption mechanism controls the uptake of CR. The pseudo-nth-order constant "n," which provides information on the reaction order, and a smaller n value of 2.161 suggests that the rate of reaction of the reactant concentration is likely to change. The smaller K_n value of 0.0322 indicates a slower reaction rate. This outcome is in agreement with the prediction of the K_1 parameter of pseudo-first order, which confirms a slow adsorption process. The h_o constant of pseudo-first and second order calculates the initial adsorption rate, and 2.339 of PFO and 6.383 of PSO obtained theoretically concur with the experimental data. The qe values of the PFO, PSO, PNO, and Avrami models, as tabulated in Table 3, were in agreement with those of the experimental data. In the Elovich model, parameter B is the desorption constant (Malash and El-Khaiary, 2010). The B value of 0.427 indicates that the adsorption of CR onto HIC is almost irreversible. The higher A value of 172.5 suggests a faster initial

adsorption rate, meaning that HIC has a high affinity for CR dye. This outcome concurs with the initial first step of the adsorption process, the "external surface adsorption or a rapid initial adsorption," as classified by Weber-Moris.

3.8.1 Error function statistical analysis

The best fit of the studied model for the uptake of CR dye on HIC was evaluated using the error parameters of the non-linear regression expression of equations 24-31 for equilibrium and kinetic model assessment. In non-linear regression, the rule for goodness-of-fit assessment is that the smaller the obtained value of the error function, the better the curve fits. The obtained results of the studied error functions for equilibrium and kinetic models, as tabulated in Table 3, show that the best fit using RMSE for the models follows the order Freundlich < Langmuir < D-R < R-P< Jovanovic < Temkin, and the best fit using x^2 for the models follows the order Langmuir < Freundlich < Jovanovic. The x^2 error parameter, as shown in Table 3, cannot describe the assumptions of the D-R, R-P, and Temkin models. The best fit using NSD and ARE for the models follows the order R-P < Temkin < Freundlich < Langmuir < Jovanovic < D-R. The error analysis of the kinetic data for the models as observed in Table 3 shows that the best fit using RMSE for the models follows the order PFO < Avrami < PNO < Elovich <PSO < FP, the best fit using NSD for the models follows the order PNO < Avrami < PFO < PSO < Elovich < FP, the best fit using x^2 for the models follows the order Avrami < PFO < Elovich < PNO < PSO < FP, the best fit using ARE for the models follows the order Avrami < PFO < PNO < PSO < FP, While the ARE cannot describe the assumptions of the Elovich model. The values of error functions EABE, HYBRID, SSE, and MSE were all high for both equilibrium and kinetic data assessment, and the reasons for these were highlighted as follows for each error function.

The high values obtained for the EABE error function may be attributed to the nature of the absolute error because it treats all deviations equally without considering their direction or magnitude. The high value of the HYBRID error function is because it combines the absolute and squared errors, which makes it more sensitive to outliers and larger deviations. The high value obtained for the SSE error function is primarily a result of the squaring of the errors, which amplifies larger deviations. The high value of the MSE error function may be attributed to the squaring of the differences between the predicted and actual values because squaring the errors accentuates larger deviations, thereby making even a small number of large errors contribute significantly to the overall MSE.

3.9 Adsorption Mechanism

3.9.1 Intra-particle diffusion model

The intra-particle diffusion model was proposed by Weber-Moris to identify the adsorption mechanism and predict the rate-controlling step. This model usually includes three steps. The first step is external surface adsorption, or boundary layer diffusion. The second step is the gradual stage of adsorption, which is intra-particle diffusion. The third step is the final equilibrium stage, in which the intra-particle diffusion starts to slow down due to the extremely low dye concentration left in the solution. However, if the data exhibit multi-linear plots, then two or more steps influence the sorption process. The intercept of the linear plot of qt versus $t^{1/2}$ in (mg/g) signals an idea about the thickness of the boundary layer, and the larger the value of the intercept, the greater the boundary layer effect (Srivastava *et al.* 2006). If the plot is linear and passes through the origin, then intra-particle diffusion is the rate-controlling step. The intra-particle diffusion model can be expressed as follows:

$$q_t = K_{id}\sqrt{t} \tag{34}$$

Where q_t (mg/g) is the amount of adsorbate adsorbed at time t, and k_{id} ($mgg^{-1}min^{1/2}$) is the intraparticle constant obtained from the slope of q_t versus $t^{1/2}$.

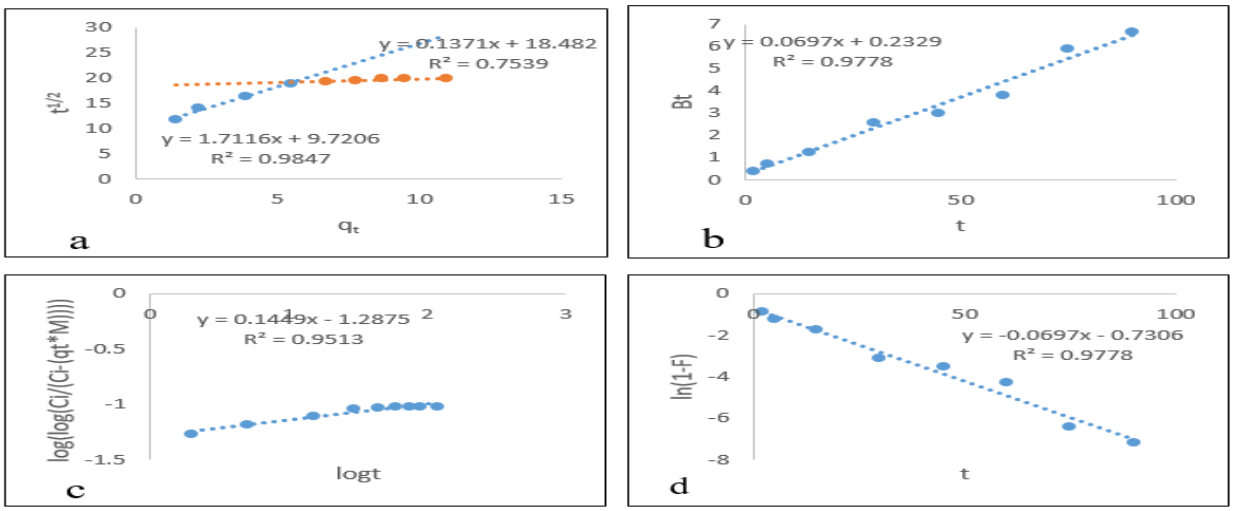

Figure 8. Adsorption mechanism plot of different models (a) Intra-particle diffusion plot, (b) Boyd diffusion model plot, (c) Bangham model plot, and (d) Liquid film model plot.

Fig. 8a shows that the linear plot did not pass through the origin, which indicated that the intra-particle diffusion was not the only rate-controlling step and that the boundary layer diffusion controlled the adsorption to some degree (Cheung *et al.* 2007). This deviation may be due to the difference in mass transfer rate in the initial and final stages of adsorption (Hameed and Hakimi 2008). Furthermore, the data, as seen in Fig. 8a, exhibit multi-linear plots, which indicate that two or more steps influence the sorption process. Comparing the k_{id} values for the macropore and micropore diffusion stages for CR uptake shows that the rate-limiting step is the micropore diffusion stage because the micropore diffusion constant $k_{id}2$ value of 0.1371 is lower than the macropore diffusion constant $k_{id}1$ value of 1.7116. This outcome confirmed the rate of micropore diffusion as the slower step and the rate-determining step. Moreover, the higher value of $k_{id}1$ also indicates that the uptake of CR onto HIC was primarily controlled by the intraparticle diffusion model. The boundary layer effect, i.e., the intercept of the micropore diffusion stages from Figure 8a, is 18.482, which further shows a greater effect than the macropore stage with an intercept of 9.7206. The non-zero intercept of the macropore diffusion stage and the micropore diffusion stage clearly shows that intra-particle diffusion is not the slowest of the rate processes that determine the overall order; thus, it can be stated that the intra-particle diffusion process is not the rate-limiting step occurring during the sorption of CR onto HIC.

3.9.2 Boyd pore model

The Boyd model is an empirical equation that also gives insight into the mechanism of adsorption. This model is applied to determine the rate-controlling step (the slow step involved) for the adsorption process. The Boyd model can be expressed as follows:

$$F = 1 - \left(\frac{6}{\pi^2}\right) exp^{(-Bt)} \quad (35)$$

$$Bt = -0.4977 - \ln(1 - F) \quad (36)$$

Where *Bt* is the function of *F* and *F* is the fraction of solute adsorbed at different times, *t*. The *Bt* values at different contact times, *t*, can be evaluated using equation (37) in the case of $F > 0.85$. The *F* value can be calculated using equation 26.

$$F = \frac{q_t}{q_e} \quad (37)$$

Where q_t and q_e are the amount of dye adsorbed on the adsorbent at any time *t* and at equilibrium respectively.

Cáceres-Jensen *et al.* (2013) proposed that if the plot of *Bt* versus *t* is a straight line and passes through the origin, it is the pore diffusion that controls the rate of mass transfer (or particle diffusion mechanism). In contrast, if the plot is

nonlinear or linear but does not pass through the origin, film diffusion or external mass transport will be the major dominating factor (Cáceres-Jensen *et al.* 2013).

Fig. 8b shows that the Boyd plot is linear but did not pass through the origin, which demonstrated that intra-particle diffusion was not the solely controllable process and that diffusion-chemisorption might be more rational to explain the adsorption of CR dye ions on HIC.

3.9.3 Bangham pore diffusion model

The Bangham pore diffusion model is an empirical model that investigates the adsorbate pore diffusion activities and it does so by calculating whether pore diffusion controls or dominates the adsorption process. The Bangham model can be expressed as follows:

$$Log\ Log\left(\frac{C_i}{C_i - q_t M}\right) = Log\left(\frac{K_J M}{2.303V}\right) + \alpha Log t \quad (38)$$

Where C_i, is the initial concentration (mg/L), V (mL) is the volume of the solution, M is the mass of the adsorbent (g), q_t is the amount of adsorbate adsorbed at time t. K_J and α are Bangham pore constants which can be obtained from intercept and slope of the plot of Log(Log(Co/(Co-(Qt*M)))) versus Log t (double logarithm plot).

Fig. 8c shows that the Bangham plot gives a nonlinear curve for the dye removal, indicating that the diffusion of adsorbate into the pores of the adsorbent is not the only rate-controlling step. Additionally, the nonlinear curve indicates multiple adsorption stages, which validates the intra-particle diffusion model that has previously indicated that two or more steps influence the sorption process. The coefficient of determination value of 0.9513 obtained from the Bangham model suggests that pore diffusion was involved in CR uptake onto HIC, and the non-linearity of the plot certifies that adsorbate pore diffusion was involved in the adsorption process.

3.9.4 Liquid film diffusion model

The Liquid film diffusion model was also used in this study to investigate if the transport of dye from the liquid phase up to the solid phase boundary also plays a role in the adsorption process. The Liquid film diffusion model can be expressed as follows:

$$-\ln(1 - F) = -K_{fd} t \quad (39)$$

Where F is the fraction of solute adsorbed at equilibrium, K_{fd} is the liquid film diffusion constant, and the F value can be evaluated using

$$F = \frac{q_t}{q_e} \quad (37)$$

Where q_t and q_e are the amount of dye adsorbed on the adsorbent at any time *t* and equilibrium respectively.

A linear plot of ─ ln (1─F) versus t with zero intercept would suggest that the kinetics of the sorption process was controlled by intra-particle diffusion through the liquid surrounding the solid sorbent.

Fig. 8d shows that the intercept of the liquid film plot of 0.7306 confirms the significance of liquid film diffusion as the major rate determination of the adsorption process since the kinetics is diffusion-limited (Srivastava *et al.* 2006). Additionally, the higher value of the liquid film coefficient of determination (R^2) value of 0.9778 indicates that film diffusion was involved as the major rate-determining step process but not the rate-determining step. This outcome concurs with the result of the Boyd model as stated earlier. Moreover, the liquid film diffusion rate constant (K_{fd}) value of -0.0697 is insignificant compared with 1.7116 of the intra-particle rate constant (k_{id}), which also confirms that the liquid film diffusion process was not the rate-limiting step occurring during the sorption of CR on HIC.

3.9 Thermodynamic Study

The variation of dye removal efficiency with temperature shall be explained by the thermodynamic parameters, such as ΔG^o, ΔH^o and ΔS^o (Hu *et al.* 2010), which are evaluated from Eqs. (16- 18). The plot of In K_C versus T^{-1} of the CR adsorption process is carried out as indicated in Fig. 9b, in which the slope and intercept obtained by a curve-fitting program are used to calculate the ΔH and ΔS.

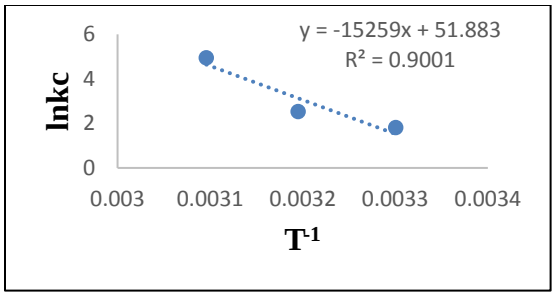

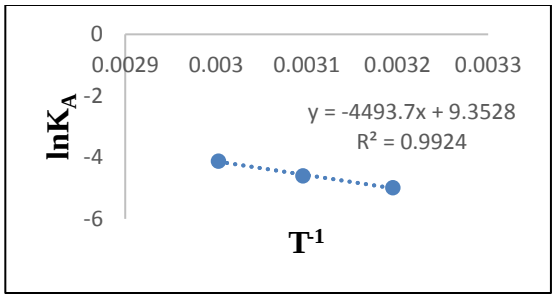

Fig.9a and b, Plot of InK_A and InK_c against T^{-1} for the removal of CR by clay adsorbent

The slope of the plots is equal to -ΔH°/R and its intercept is equal to ΔS°/R. The calculated parameters of ΔG, ΔH, and ΔS are shown in Table 4.

Table 4 Thermodynamics parameters for the adsorption of CR on HIC

Temp (K)	InK_c	ΔG (KJ/MOL)	ΔS (J/MOL)	ΔH (KJ/MOL)	E_a (KJ/MOL)
303	1.8144	-4.87248			
313	2.5332	-6.80272	431.3553	126.863	37.3606
323	4.9418	-13.2977			

The negative values of ΔG indicate that adsorption is spontaneous, the positive value of ΔH indicates that the adsorption process is endothermic, and the positive value of ΔS suggests increased randomness at the solid or solution interface during the adsorption of CR on HIC and corresponds to an increase in the degree of freedom of the adsorbed species (Dalia *et al.* 2011). Thus, adsorption is favored on CR. Reddy *et al.* (2011) reported a similar phenomenon in the removal of Congo red from an aqueous medium using jujube seed.

3.9.1 Activation Energy

The magnitude of the activation energy yields information on whether the adsorption is mainly physical or chemical. The physisorption process normally had an activation energy of 5–40 KJ/mol, while chemisorption had a higher activation energy (40–800 KJ/mol) (Wu, 2007). To evaluate the activation energy of adsorption, the Arrhenius equation was applied using the relationship of Eqs. 19.

Fig. 9a shows the plot of the activation energy of CR on the HIC adsorbent, and Table 4 presents the calculated Ea values for the adsorption.

It is observed from Table 4 that the E_a value for CR adsorption on HIC is positive and below 40 KJ mol^{-1}, thus indicating that adsorption of CR using HIC is feasible and a physisorption process. This phenomenon concurs with the Freundlich constant "n_f" result, which refers to the process as physical. A similar phenomenon was reported on the adsorption of basic dye using acid-treated kenal fiber char (Dalia *et al.* 2011).

3.10 Optimization Using Response Surface Methodology

3.10.1 ANOVA analysis for CR removal

The Design expert was used to analyze the result and the summary of the P-value and the model summary statistics are presented in Table 5.

Table 5: Statistical summary of the models investigated

Source	Df	Standard deviation	R-squared	Adjusted R^2	Predicted R^2	PRESS
Linear	40	2.91	0.6529	0.5974	0.5187	292.68
2FI	14	3.12	0.6952	0.5348	0.0563	573.88
Quadratic	10	0.7566	0.9859	0.9727	0.9013	60.02
Cubic	2	0.2492	0.9993	0.9970	0.8502	91.09

The quadratic model for optimum point prediction of the process was suggested from the CCD module with high R-squared values of 0.9859, adjusted R^2 values of 0.9727, and predicted R^2 values of unity 0.9013. Table 6 presents the analysis of variance (ANOVA) and it confirms the adequacy of the quadratic model.

Table 6: ANOVA and model coefficients for CR adsorption

Source	Sum of squares	Df	Mean squares	F-value	p-value Prob>F
Model	599.52	14	42.82	74.81	< 0.0001
B-Temperature	21.88	1	21.88	38.22	< 0.0001
A-Concentration	106.18	1	106.18	185.48	< 0.0001
D-pH	246.76	1	246.76	431.06	< 0.0001
C-Particle size	22.24	1	22.24	38.36	< 0.0001
AB	6.45	1	6.45	11.27	0.0043
AC	0.0012	1	0.0012	0.0021	0.9637
AD	0.9801	1	0.9801	1.71	0.2104
BC	0.2401	1	0.2401	0.4194	0.5270
BD	5.98	1	5.98	10.44	0.0056
CD	12.04	1	12.04	21.03	0.0004
A^2	13.51	1	13.51	23.60	0.0002
B^2	25.90	1	25.90	45.24	< 0.0001
C^2	0.9156	1	0.9156	1.60	0.2253
D^2	62.40	1	62.40	109.01	< 0.0001
Residual	8.59	15	0.5724		
Lack of fit	8.59	10	0.8587		
Pure error	0.0000	5	0.0000		
Cor total	608.10	29			

Significant terms of the model are checked from F-values and P-values. The higher the F-value, the smaller the P-value, and the more significant the corresponding coefficient. The higher model F-value of 74.81 implies that the model is significant, and P-values less than 0.0500 indicate model terms are significant; therefore, A, B, C, D, AB, BD, CD, A^2, B^2, and D^2 are significant terms. A similar phenomenon was reported by Amini *et al.* (2008). The empirical correlation between the variables (response and independent) in the coded form based on the experiment results was reported as follows:

$$\% \text{ Adsorbed} = 97.90 - 2.30A + 1.05B - 1.05C - 3.51D - 0.6350AB + 0.6113BD + 0.8675CD - 1.20A^2 - 1.67B^2 - 2.59D^2 \quad (40)$$

The good fit of the model equation was validated using R^2 (coefficient of regression). The high coefficient of regression value of 0.9859 implies that 98.59% of the variability in the response can be explained by the model.

3.10.2 RSM graphical plots

This plot shows the relationship between the actual and predicted values of the response. As seen in Fig. 10, all the data points are assembled into the straight line of the coefficient of regression of 0.9859, which signifies a good correlation between the actual and predicted values of the response. The coefficient of regression of 0.9859 certifies that the prediction of the quadratic model is correct in describing the removal of dye from an aqueous solution. A similar phenomenon was reported by Iheanacho *et al.* (2019) and Onu and Nwabanne (2014).

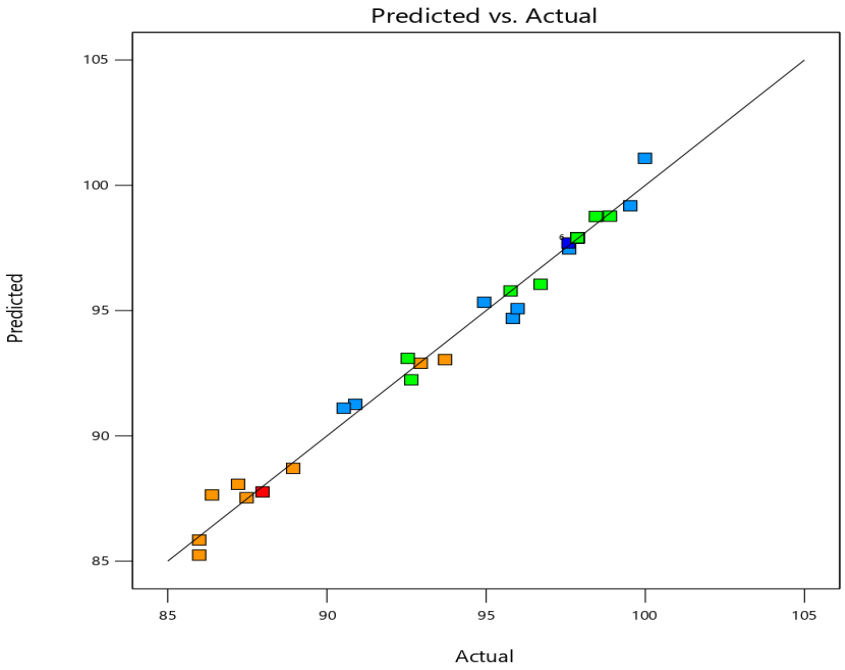

Fig 10: Plot of the experimental and predicted response

The 3D surface plots represent the effect of two process variables on the adsorption of CR. Fig.11a-b, presents the relationship between every two independent process variables. The circular nature of the contour in the graphs shows that there was a perfect significance between every two variables.

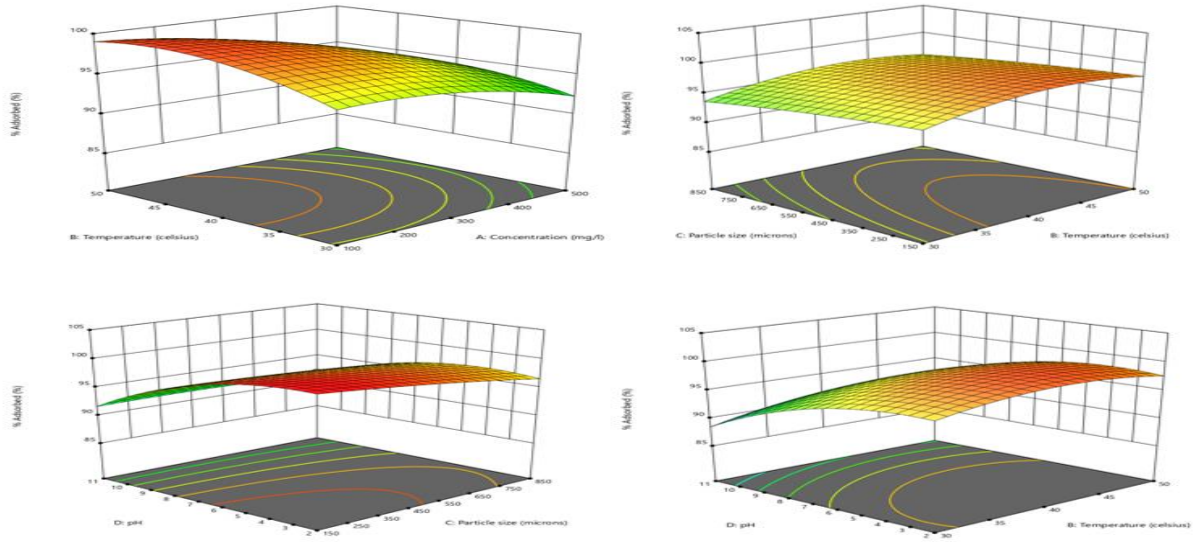

Figure 11: 3D surface plot for CR adsorption on the adsorbent showing combined effects of (a) Time and pH, (b) Temperature and concentration

3.11 ANN Modeling and Prediction

The artificial neural network for the adsorption of CR was modeled using the neural toolbox of MATLAB software. The best ANN with input, hidden, and output nodes of 4, 9, and 1, respectively, was used to model the optimum percentage removal of CR in the adsorption process. The input nodes represent the independent variables, while the output nodes represent the response. The hidden layers show the nonlinear transformations in the input space. The optimal number of neurons in the hidden layer was determined by varying the number of neurons in the hidden layer and comparing the mean square error obtained. Therefore, the ANN topology architecture of 4-9-1, corresponding to the four input variables (temperature, concentration, pH, and adsorbent dosage), nine neurons in the hidden layer, and one output variable (percentage adsorbed), was used in the ANN modeling. Levenberg-Marquardt (LM) backpropagation was the algorithm utilized in the ANN modeling. The properties of ANN modeling are algorithm, error function, input layer neuron, hidden layer neuron, output layer neuron, training, hidden layer, and data division.

The validation of the neural network process at the 6th epoch iteration was achieved using the ANN validation performance plot in Figure 12, and the lowest mean square error of 3.4675×10^{-21} was observed.

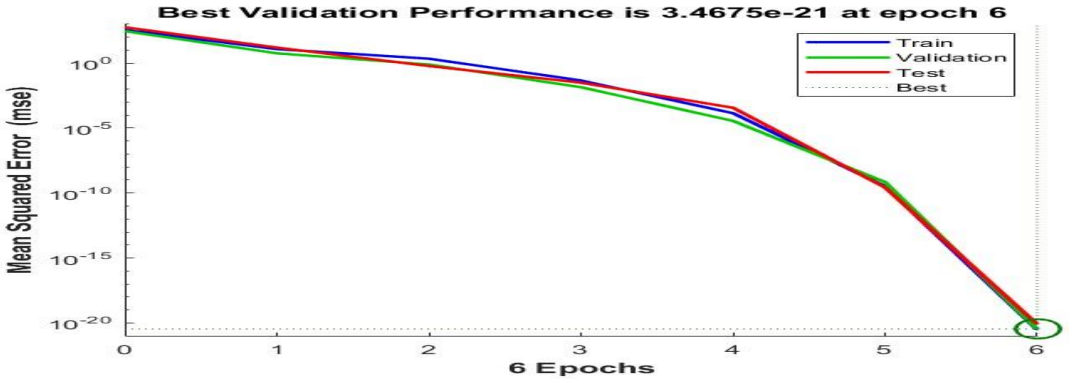

Figure 12: ANN validation performance plot

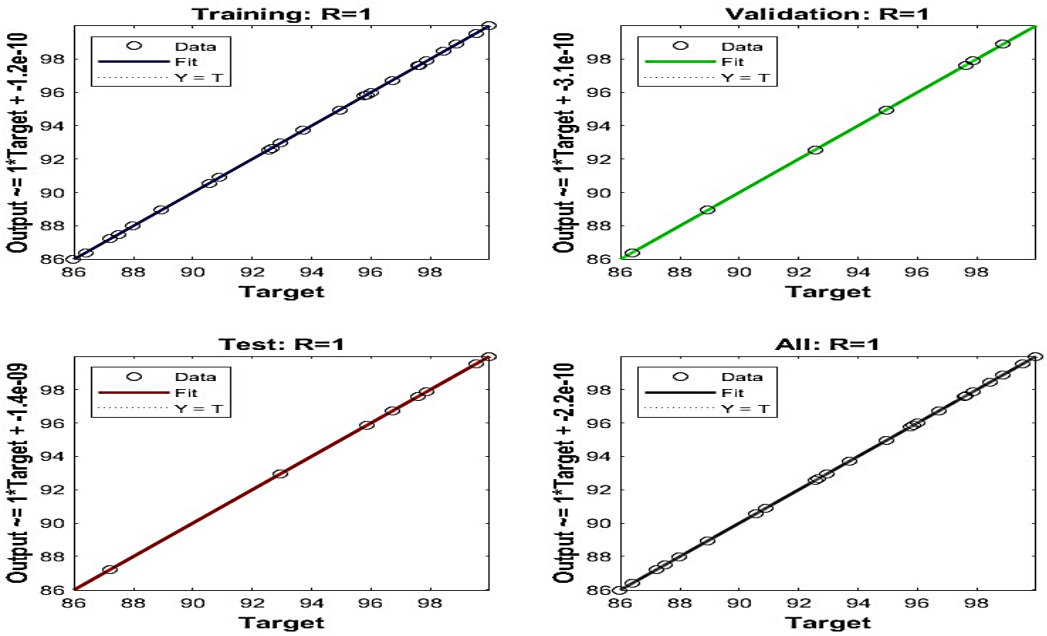

Figure 13: ANN regression plots for (A) training, (B) test, (C) validation and (D) overall process

The experimental data were divided into training, testing, and validation so that the number of parameters in the model would not exceed the size of the training dataset. Scatter diagrams that compare experimental data (target) with computed neural data for training, testing, validation, and overall data are shown in Figure 13. The regression values of unity were obtained for the training, testing, validation, and all (overall) data, respectively. These coefficients of regression values of unity explain the nature of the neural fittings. Moreover, the outputs were very close to the targets, as most of the data points were assembled along the straight line of the coefficient of regression. The percentage predicted CR removal of the ANN model is presented in Table 7.

3.12 ANFIS Modeling and Prediction

Four input parameters (temperature, concentration, pH, and adsorbent dosage) were utilized to predict the percentage of CR dye removal using the ANFIS model. Figure 14 shows the ANFIS Sugeno diagram.

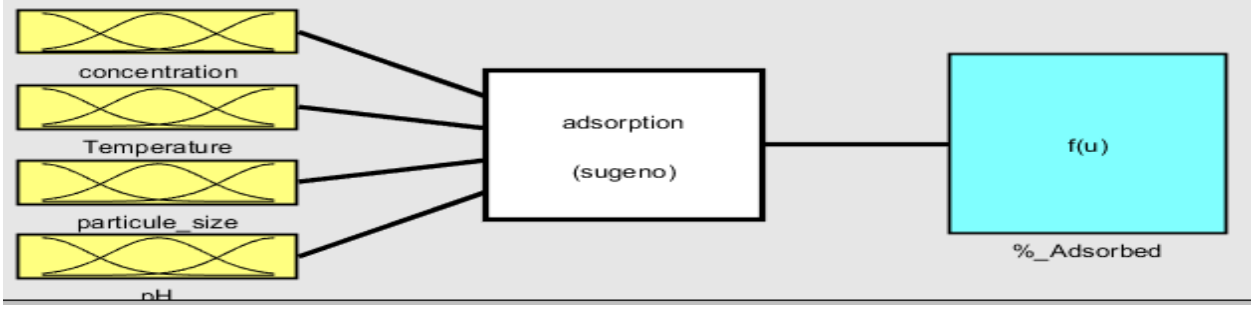

Figure 14: ANFIS Sugeno diagram of CR adsorption process

A 30x5 matrix (representing the input variables) and a 30x1 matrix (representing the output variable) were used in the MATLAB m-file. The Gaussian combination membership function (Guass2mf) was employed in checking the grid partition. Three membership functions were assigned to each input layer in generating the FIS. The ANFIS data was trained at 5 epoch iterations with an error tolerance of zero. A minimum error of 0.000229327 was produced after the

2nd epoch, which gives reliance on the adequacy of the ANFIS model in predicting the removal of CR dye. A plot of FIS against training data is shown in Figure 15. A hybrid learning algorithm that makes use of the gradient method and the least squares method was used in optimizing the ANFIS model. A correlation coefficient of 0.9999 confirms the adequacy of the ANFIS model in predicting the removal of CR dye from wastewater using Ihiala clay.

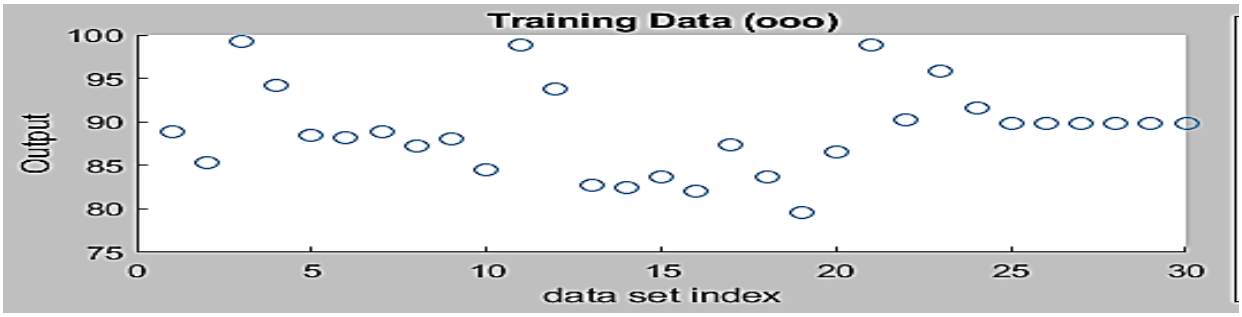

Figure 15: Plot of FIS against training data of CR adsorption

3.13 Comparison of Experimental Response with Predicted Response of RSM, ANN, and ANFIS models

Table 7: Experimental and predicted results for CR removal

Conc(mg/l)	Temp(^{0}c)	P.size (μm)	pH	Actual Resp	RSM Pred	ANN Pred	ANFIS Pred
300	40	500	0.136039	97.59	97.7	97.59	97.5898
100	30	850	2	95.99	95.08	95.99	95.9896
500	50	850	11	87.48	87.53	87.48	87.4797
300	40	500	6.5	97.87	97.9	97.87	97.86998
100	30	150	2	99.53	99.18	99.53	99.5297
500	50	150	11	86.39	87.65	86.39	86.3897
300	40	500	6.5	97.87	97.9	97.87	97.86998
300	40	500	6.5	97.87	97.9	97.87	97.86998
100	50	150	2	99.99	101.08	99.99	99.9897
500	50	850	2	90.53	91.11	90.53	90.5297
300	40	500	12.864	87.98	87.77	87.98	87.9799
300	40	500	6.5	97.87	97.9	97.87	97.86998
500	50	150	2	95.84	94.69	95.84	95.8397
500	30	850	11	85.99	85.24	85.99	85.9897
100	50	850	11	92.95	92.9	92.95	92.9497
100	50	850	2	97.61	97.46	97.61	97.6097
500	30	150	2	94.94	95.33	94.94	94.9397

300	54.1421	500	6.5	96.71	96.05	96.71	96.7098
500	30	150	11	85.99	85.85	85.99	85.9897
300	40	994.975	6.5	95.77	95.79	95.77	95.7698
500	30	850	2	90.89	91.26	90.89	90.8897
300	40	5.02525	6.5	98.89	98.77	98.89	98.8898
100	30	850	11	87.21	88.07	87.21	87.2097
582.843	40	500	6.5	92.65	92.24	92.65	92.6499
300	40	500	6.5	97.87	97.9	97.87	97.86999
100	50	150	11	93.71	93.05	93.71	93.7097
17.1573	40	500	6.5	98.45	98.76	98.45	98.4498
300	25.8579	500	6.5	92.54	93.09	92.54	92.5399
300	40	500	6.5	97.87	97.9	97.87	97.86999
100	30	150	11	88.94	88.71	88.94	88.9397

The result showed that the three models were good at modeling and predicting the removal of CR from wastewater in an adsorption process. RSM with the lowest residuals in most experimental data sets seems to be the best at predicting the percentage of CR removed. Further statistical analyses were used to compare the adequacy of the three models in Table 8.

Table 8: Comparative statistical analysis of RSM, ANN, and ANFIS models

Model parameter	RSM	ANN	ANFIS
R^2	1	1	1
ARE	2.36×10^{-5}	7.41×10^{-14}	7.07×10^{-6}
HYBRID	1.42×10^{-7}	1.40×10^{-24}	1.27×10^{-8}
RMSE	7.14×10^{-4}	2.24×10^{-12}	2.14×10^{-4}
SSE	0.0004	3.94×10^{-21}	3.58×10^{-5}
MSE	1.43×10^{-5}	1.41×10^{-22}	1.28×10^{-6}
NSD	2.4×10^{-5}	7.67×10^{-14}	7.31×10^{-6}
EABE	0.02	6.28×10^{-11}	0.00598

The model parameters investigated include R^2, APE, HYBRID, RMSE, SSE, MSE, NSD, and EABE. In the model indices, RSM showed the least modeling predictive ability in all of the studied error functions used for the comparative analysis, whereas the ANN exhibited the best modeling predictive ability in all of the studied error functions used for the comparative analysis.

3.14 Comparative Performance of the Adsorbent

A comparison of the adsorption of Congo red dye with other adsorbents was made to ascertain the efficiency and relevancy of the modified clay used in this study. Maximum adsorption capacity (q_{max}), percentage removal, and adsorbent dosage were the parameters utilized in the comparison, as shown in Table 9.

Table 9: Comparison with other adsorbents

Adsorbent	Adsorbent dos (g)	Removal eff (%)	Ads capacity (mg/g)	Adsorbate	Reference
Pottery clay	0.05	94.75	1.086	Congo red	Baydaa and Lekaa (2022)
Koura clay	0.05	82.95	0.224		
MgAl-LDH	0.05	60	769.23	Congo re	Mohamed *et al.* (2022)
PDFe/Al	1	99	411	Congo red	Khathutshelo *et al.* (2022)
Activate glHIConite	0.02	80	11.9	Congo red	Hamd *et al.* (2023)
Treated clay	0.3	90	39.80	Heavy metals	Paul and Mutsee (2021)
Activated carbon	1	92.45	84.46	Congo red	Akande *et al.* (2023)
Agricultural waste (raw)	3.5	-	55.56	Congo red	Jegede *et al.* (2021)
Agricultural waste (modified)	1.5	-	58.48		
Modified red clay (MRC)	0.1	85	181.818	Methylene blue	Carazeanu *et al.* 2023
Banana stem	0.5	87	14.28	Remazole red	Kumar *et al.* (2022)
Rice bran	2	97.4	603	Crystal violet	Mojtaba *et al*. (2020)
Fe-bent	2	99	10.06	Arsenic(v)	Barakan *et al.* (2019)
Bentonite	1	95.21	151.5	Cr(III)	Amir *et al.* (2020)
	1	95.74	161.3	Cr(VI)	
Modified clay	1	99.3	86.7	Congo red	Present study

From Table 9, it can be seen that the adsorption capacity and removal efficiency of the modified Ihiala clay were higher than some of the reviewed adsorbents. The availability of this clay in large deposits in Ihiala town, Nigeria with its adsorption efficiency makes it a viable effective and alternative adsorbent in the removal of Congo red dye from contaminated water.

Table 10 Comparison of parameters of untreated and treated simulated industrial wastewater containing CR dye after 24hrs incubation

Parameters	Wastewater	Treated Wastewater	% Removal
EC (µs/cm)	101	21.7	78.51
TDS (mg/l)	51	5.1	90
COD (mg/l)	169	27	84.02
Color removal (mg/l)	100	0.7021	99.3

Table 10 presents the adsorption capacity and removal efficiency of the HIC in minimizing contamination of dye industrial wastewater. The result shows a high reduction rate of the tested parameters after treatment, which thereby confirms HIC as a reliable adsorbent for industrial wastewater treatment. The obtained result is in agreement with the previous report by Mustafa *et al.* (2023), who reported that the biosynthesis of nickel oxide nanoparticles removes 48.38% of EC, 49.24% of COD, and 67.05% of TDS from Azo Dye Industrial Wastewater.

3.15 Regeneration of Adsorbent

The desorption capacity of the adsorbent is presented in Fig. 16a–c. Fig. 16a presents the effect of different pH on two different eluents (alkaline eluent and acidic eluent) after four desorption cycles. The result shows that CR dye desorption works perfectly with alkaline eluent due to the electrostatic repulsion that exits when the OH-ion of NaOH neutralizes the H^+ ion on the surface of the adsorbent. The highest desorption capacity of 88% was achieved at pH 10 after four successive regeneration cycles, against 26.1% at pH 12. This high desorption capacity at pH 10 instead of pH 12 is attributed to high alkalinity strength, which may weaken both the chemical and pore structures of the adsorbent surface and thereby lead to poor outcomes. Fig. 16b presents the effect of five different eluent concentrations (0.5M, 1M, 2M, 4M, and 5M) on the desorption process.

The obtained result shows that low and higher concentrations did not favor the process, since 89.3% desorption capacity was recorded at 2M concentrations against 75.7% at 4M and 60.6% at 1M concentrations after four successive desorption cycles. The slow rate of desorption at 1M is attributed to a weak driving force and thus requires a larger volume of eluent to achieve the same objective as with mid-concentrated eluent, whereas the low desorption rate at higher concentrations is due to the adverse effect of eluent high concentration strength, which may destabilize or weaken the chemical and pore structure of the adsorbent. Fig. 16c presents the effect of three different temperatures (303 k, 313 k, and 323 k). The result indicates that temperature did not have a significant effect on the desorption process since 88.9%, 89.5%, and 90.7% were achieved for temperatures 303k, 313k, and 323k after four successive desorption cycles; therefore, it is obvious that low temperatures pose the benefit of cost efficiency since the difference between the results at 303k and 323k is insignificant.

Finally, Fig. 10 shows an insignificant change in desorption capacity between the 2^{nd} and 4^{th} desorption cycles, irrespective of whether the 4^{th} was the best. This observed minor change in desorption capacity between the 2nd and 4^{th} cycles is attributed to characteristics of equilibrium. The obtained result is in agreement with the previous report by Zhang *et al.* (2018), who reported that temperature has an insignificant effect on the desorption of the five synthetic azo dyes (tartrazine, amaranth, carmine, sunset yellow, and Allura red). They also reported that optimized desorption efficiency was achieved at pH 9. Wang *et al.* (2020) reported similar results with the same trend on effect concentration. Himanshu (2021) reported that alkali eluents are best used for anionic adsorbates.

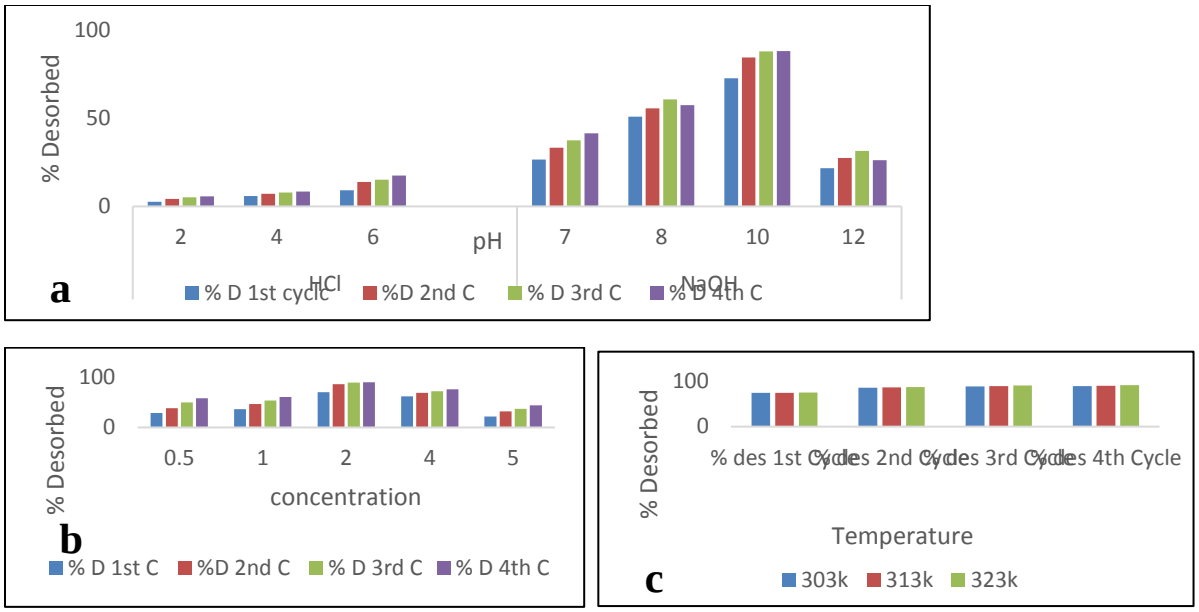

Figure 16: Effect of pH, concentration, and temperature of eluent on desorption of CR on HIC

4.0 CONCLUSIONS

The present study established the potential of HIC as an adsorbent for the removal of dye from aqueous solutions. The adsorption of CR onto HIC was found to be dependent on the pH solution, initial dye concentration, temperature, adsorbent dosage, contact time, and adsorbent particle size. The equilibrium adsorption data was best represented by the V-S isotherm model. The Langmuir model produced the highest maximum adsorption capacity (q_{max}) value of 86.70 mg/g. The adsorption kinetics are best described by Avrami kinetic models. From the thermodynamic studies, the adsorption process was spontaneous, endothermic, favorable, and physical, and this was in agreement with the findings of the equilibrium adsorption parameters. The ANN, ANFIS, and RSM models were adequate for predictive modeling of the adsorption process, though the statistical analysis indicated that the RSM model was marginally better than the ANN and ANFIS.

References

Adebayo M.A, Jabar J.M, Amoko J.S, Openiyi E.O, and Shodiya O.O. 2022. Coconut husk-raw clay-Fe composite: preparation, characteristics and mechanisms of Congo red adsorption. *Sci Rep*. 2022 Aug 23;12(1):14370. doi: 10.1038/s41598-022-18763-y.

Aharoni, C. and Ungarish, M. 1977. Kinetics of activated chemisorption. Part 2.-Theoretical models *J. Chem. Soc*., Faraday Tran., 73(1), 456-464. http://dx.doi.org/10.1039/f19777300456

Akande, J.A, Adeogun A.I, Uzosike A.S. 2023. Removal of Congo Red Dye from Simulated Wastewater Using Activated Carbon Derived from Corn Cobs; Kinetics and Equilibrium Studies, *Global Journal of Pure and Applied Chemistry Research*, Vol.11, No.1, pp.1-19

Amini A, Younesi H, Bahramifar N, Lorestani A,Ghorbani F, Daneshi A and Sharifzadeh M. 2008. Application of Response Surface Methodology for Optimization of Lead Biosorption in an Aqueous Solution by Aspergillusniger. *J. Hazard. Mater*, 154, 694-702.

Amir A, Rauf F, Hossein E, and Sajad T. 2020. The role of bentonite clay and bentonite clay@MnFe2O4 composite and their physico-chemical properties on the removal of Cr(III) and Cr(VI) from aqueous media. *Environ Sci Pollut Res* https://doi.org/10.1007/s11356-020-07756-x

Arana J.M.R.R., and Mazzoco R.R. 2010. Adsorption studies of methylene blue and phenol onto black stone cherries prepared by chemical activation, *J. Hazard. Mater*. 180 (2010) 656–661. Doi:10.1016/j.jhazmat.2010.04.086.

Arulkumar, M., Sathishkumar, P., Palvannan, T. 2011. Optimization of orange G dye adsorption by activated carbon of thespesiapopulnea pods using response surface methodology. *Journal of Hazardous Materials.* 186 (1), 827–834. https://doi.org/10.1016/j.jhazmat.2010.11.067.

Avrami M. 1939. Kinetics of phase change. I. General theory. *The Journal of Chemical Physics* 7(12):1103-1112.

Bahman N and Sina F.A. 2018. Application of ANFIS, ANN, and logistic methods in estimating biogas production from spent mushroom compost (SMC). *Resources, Conservation & Recycling* 133 169–178 https://doi.org/10.1016/j.resconrec.2018.02.025 Langmuir I. 1916. The constitution and fundamental properties of solids and liquids. *J. AM. Chem. Soc*. 38(11), 2221-2295. Doi.org/10.1021/ja02268a022.

Barakan S, Aghazadeh V, Samiee B. A, Mohammadi S. 2019. Thermodynamic, kinetic and equilibrium isotherm studies of As(V) adsorption by Fe(III)-impregnated bentonite. *Environ Dev Sustain*. https://doi.org/10.1007/s10668-019-00424-2

Baydaa N. A, and Lekaa H. K. 2022. Removal of Congo Red Dye from Aqueous Solution Using Different Clays Adsorbent. *Journal of Algebraic Statistics* Volume 13, No. 3, 2022, p. 861 - 875 https://publishoa.com ISSN: 1309-3452 861

Bhattacharyya K.G., and Sharma A. 2005. Kinetics and thermodynamics of methylene blue adsorption on Neem (Azadirachta indica) leaf powder, *Dyes Pigments* 65 51–59. Doi:10.1016/j.dyepig2004.06.016

Boyd, G.E., Adamson, A.W., Meyers Jr., L.S. 1947. The exchange adsorption of ions from aqueous solutions by organitezeolithes. II. Kinetics. *J. Am. Chem. Soc*. 69, 2836.

Cáceres-Jensen L., Rodríguez-Becerra J., Parra-Rivero J., Escudey M., Barrientos L, and Castro-Castillo V. 2013. Sorption kinetics of diuron on volcanic ash derived soils. *Journal of Hazardous Materials*. 2013;261: 602–613. doi: 10.1016/j.jhazmat.2013.07.073.

Carazeanu P.I., Roscaa. I, and Dumbravaa. A. 2023. Modified red clays as adsorbents in the removal of cationic dyes from aqueous solutions. *Digest Journal of Nanomaterials and Biostructures* Vol. 18, No. 2, April - June 2023, p. 567 – 578

Cheung, W. H., Szeto, Y. S.; and Mckay, G. 2007.Intraparticle diffusion processes during acid dye adsorption onto chitosan. *Bioresour.Technol*. 98(15), 2897-2904. Doi.org/10.1016/j.biortech.2006.09.045

Dal S. K, and Meenal G. 2022. Treatment of Textile Dyeing Effluent Using Agriculture Waste Based Adsorbents - A Review. *Chemical Science International Journal.* Volume 32 [Issue 6] DOI: 10.9734/CSJI/2023/v32i6870

Dalal R.C.1974. Desorption of phosphate by anion exchange resin. *Commun Soil Sci Plant Anal* 5:531–538

Dalia, K. M; Mohamad, A. M. S; Wan, A. W. A. K; Azni, I, and Zurina, Z. A. 2011. Batch adsorption of basic dye using acid treated kenaffibre char: equilibrium, kinetic and thermodynamics studies. *Chem Eng. J.* 181-182, 449-457. Doi: 10.1016/j.cej.2011.11.116.

Dotto, G. L., and Pinto, L. A. A. 2011. Adsorption of Food Dye Acid Blue 9 and Food Yellow 3 onto Chitosan: stirring Rate effect in Kinetics and Mechanism. *J Hazard.Mater*. 187, 164-170.

Dubinin M.M and Radushkevich L.V. 1947. Equation of the characteristic curve of activated charcoal. *Proc Acad Sci Phys Chem* Sect USSR 55:331–333

El-Halwany M.M. 2010.Study of adsorption isotherms and kinetic models for methylene blue adsorption on activated carbon developed from Egyptian rice hull (Part II), *Desalination* 250(1) 208–213. Doi.org/10.1016/j.desal.2008.07.030.

Elovich, S.Y., Larinov, O.G. 1962. Theory of adsorption from solutions of non-electrolytes on solid (I) equation adsorptionfrom solutions and the analysis of its simplest form, (II)verification of the equation of adsorption isotherm from solutions. *Izv. Akad. Nauk. SSSR, Otd. Khim. Nauk. 2, 209–216.*

Freundlich H.M.F. 1906. Over the adsorption in solution *J. Phys. Chem.* 57, 385-470.

Gonzalez C.R.T., Subathra M.S.P., and Manoj K.N. 2020. Modelling the daily reference evapotranspiration in semi-arid region of South India: A case study comparing ANFIS and empirical models. *Information Processing in Agriculture* 2-12. https://doi.org/10.1016/j.inpa.2020.02.003.

Hamd A, Salah D, Alyafei H. F, Soliman N. K, El-Reedy A. A. M, Elzanaty A. M, Al-Saeedi S. I, Al-Ghamdi A, Shaban M, and El-Sayed R. 2023. NaOH-Activated Natural Glauconite for Low-Cost Adsorption of Congo Red Dye *Water* 2023, 15, 3753. https://doi.org/ 10.3390/w15213753

Hameed, B. H. and Hakimi, H. 2008. Utilization of durian (DurioZibethinus Murray) peel as low cost sorbent for the removal of acid dye from aqueous solutions. *Biochem.Eng.J.* 39(2), 338-343. Doi:10.1016/j.bej.2007.10.005

Himanshu P. 2021. Review on solvent desorption study from exhausted adsorbent. *Journal of Saudi Chemical Society* (2021) 25, 101302

Ho, Y.S. and McKay, G. 1999. Pseudo-Second Order Model for Sorption Processes. *Process Biochemistry*, 34, 451-465.

Ho, Y.S., Wase, D.A.J., Forster, C.F. 1996. Removal of lead ions from aqueous solution using sphagnum moss peat as adsorbent. *Water* SA 22, 219–224.

Ho, Y.S., McKay, G. 1999. Pseudo second order model for sorption process. Process *Biochem.* 34, 451–465. https://doi.org/10.1016/S0032-9592(98)00112-5

Hu, Z; Chen, H; ji, F, and Yuan, S. 2010. Removal of Congo red from aqueous solution by cattail root, *j. Hazard. Mater*. 173(1-3). 292-297. Doi.org/10.1016/j.jhazmat.2009.08.082.

Iheanacho C. O., Nwabanne J.T. and Onu C.E. 2019. Optimum Process Parameters for Activated Carbon Production from Rice Husk for Phenol Adsorption. Current Journal of *Applied Science and Technology*, 36(6): 1-11. https://doi.org/10.9734/CJAST/2019/v36i630264

Imessaoudene, A.; Cheikh, S.; Hadadi, A.; Hamri, N.; Bollinger, J.-C.; Amrane, A.; Tahraoui, H.; Manseri, A.; Mouni, L. 2023. Adsorption Performance of Zeolite for the Removal of Congo Red Dye: Factorial Design Experiments, Kinetic, and Equilibrium Studies. *Separations* 2023, 10, 57. https://doi.org/10.3390/separations10010057

Ismat A. E, Marufa K, Most. Afroza K, Owaleur R.M.d., Anis-Ul-Haque K. M., and

Jegede M. M., Durowoju O. S., and Edokpayi J. N. 2021. Sequestration of Hazardous Dyes from Aqueous Solution Using Raw and Modified Agricultural Waste. *Adsorption Science & Technology*, Volume 2021, Article ID 6297451 https://doi.org/10.1155/2021/6297451

Jovanovic, D.S. 1969. Physical adsorption of gases—II: Practical application of derived isotherms for monolayer and multilayer adsorption. *Kollozd Z.*, 235, 1214–1225.

Juraj B. 2023. Controversial Issues Related to Dye Adsorption on Clay Minerals: A Critical Review. *Molecules* 2023, *28*(19), 6951; https://doi.org/10.3390/molecules28196951

Kausar A., Bhatti H. and Mackinnom G. 2013. Equilibrium kinetic and thermodynamics studies on the removal of U (VI) by low-cost agricultural waste, *Colloids and Surface B*, Vol 111, 2013, 124-133. Doi.org/10.1016/j.colsurfb.2013.05.025.

Khathutshelo L. M., Vhahangwele M., Johannes P. M., Nils H., and Hendrik G. B. 2022. Nanotechnology in the Restoration of Polluted Soil. *Nanomaterials (Basel).* 12(5): 776. doi: 10.3390/nano12050776.

Kolmogorov A., Petrovskii I., and Piskunov N. 1937. A study of the diffusion equation with increase in the amount of substance, and its application to a biological problem. *Bulletin of Moscow University Mathematics and Mechanics* 1(6):1-26.

Kumar K. A, Bharath M, and Krishna B. M. 2022. Adsorption kinetics of reactive dye using agricultural waste: banana stem. *Water Practice and Technology* 17 (1): 128–138. https://doi.org/10.2166/wpt.2021.106

Ladhe, U. V., Wankhede, S. K., Patil, V. T., and Patil, P. R. 2011. Adsorption of Eriochrome Black-T from Aqueous Solution on Activated Carbon prepared from Mosambi Peel. *Jol.of Applied Sci. in Environmental Sanitation*, 6(2), 149-154.

Lafi R, Montasser I, and Hafiane A. 2019. Adsorption of Congo red dye from aqueous solutions by prepared activated carbon with oxygen-containing functional groups and its regeneration. *Adsorpt. Sci. Technol.* 2019;37:160–181. doi: 10.1177/0263617418819227.

Lagergren, S., 1898. Zur theorie Der Sogenannten adsorption geloster stoffe, Kungliga Svenska Vetenskapsakademiens. *Handlingar* 24, 1–39.

Lata H., Garg V., and Gupta R. 2007. Removal of basic dye from aqueous solution by adsorption using Partheniumhysterophorus: an agricultural waste, *Dye pigments* 74(3), 653-658 .doi.org/10.1016/j.dye.2006.04.007.

Mahammedi F and Benguella B., 2016. Adsorption of methylene blue from aqueous solutions using natural clay. *J. Mater. Environ. Sci. 7 (1) (2016) 285-292*

Mahmoud El O., Mohamed L., Hicham A. O., Younes B., Abdelhadi A., Abdelaziz E., Abdelaziz A. A., and Abdellatif L. 2019 Efficient removal of p-nitrophenol from water using montmorillonite clay: insights into the adsorption mechanism, process optimization, and regeneration. *Environ Sci Pollut Res* 26:19615–19631. https://doi.org/10.1007/s11356-019-05219-6

Mahmoodi M., Hayati M. B., Arami M., and Lan C. 2011. Adsorption of textile dyes on Pine Cone from colored wastewater: Kinetic, equilibrium and thermodynamic studies. *Desalination* 268(1-3), 117-125. Doi: 10.1016/j.desal.2010.10.007.

Malash, G. F., and El-Khaiary, M. I. 2010. Methylene blue adsorption by the waste of Abu-Tartour phosphate rock. *J. Colloid Interface Sci.* 348(2), 537-545. Doi: 10.1016/j.jcis.2010.05.005.

Manpreet S.B., DhritiKapoor, R.K., Kalia, A. S. R., and Ashwani K.T. 2011. RSM and ANN modeling for electrocoagulation of copper from simulated wastewater: Multi objective optimization using genetic algorithm approach. Desalination 274 (2011) 74–80. doi: 10.1016/j.desal.2011.01.083.

Mingyi, F., Tongjun, L., Jiwei, H., Rensheng, C., Xionghui, W., Xuedan, S., and Wenqian, R. 2017. Artificial neural network modeling and genetic algorithm optimization for cadmium removal from aqueous solutions by reduced graphene oxide-supported nanoscale zero-valent iron (nzvi/rgo) composites. *Materials.* 10 (544), 1 – 22. doi:10.3390/ma10050544.

Mourabet, M.E., Rhilassi, A., Bennani-Ziatni, M., and Taitai, A. 2014. Comparative Study of artificial neural network and response surface methodology for modelling and optimization the adsorption capacity of fluoride onto apatitictri calcium phosphate. *Universal Journal of Applied Mathematics*. 2(2), 84-91. doi: 10.13189/ujam.2014.020202

Mohamed A. F., Abdelfattah M. S., Hanem F. K., Noha B, Walaa A., Khadijah H. A., and Ibrahim T. R. 2022. Optimized adsorption and effective disposal of Congo red dye from wastewater: Hydrothermal fabrication of MgAl-LDH nanohydrotalcite-like materials *Arabian Journal of Chemistry* Volume 15, Issue 11, November 2022, 104171. https://doi.org/10.1016/j.arabjc.2022.104171

Mohammed B., Mustapha D., and Ftiha D. 2022. Adsorption of dye using natural clay from water. *Journal of Environmental Engineering and Science.* Volume 17 Issue 4, December 2022, pp.175-183. https://doi.org/10.1680/jenes.21.00051

Mohammed G. H., Magdy A. W., Hosni A. G., and Ahmed S. E. 2023. Adsorption of Rose Bengal dye from waste water onto modified biomass. *Sci Rep.* 2023; 13: 14776. doi: 10.1038/s41598-023-41747-5

Mojtaba R., Majid B., Naser M., and Mohammad A. A. 2020. Adsorption of crystal violet dye by agricultural rice bran waste: Isotherms, kinetics, modeling and influencing factors. *Environmental Engineering Research* 2021;26(3): 200128. DOI: https://doi.org/10.4491/eer.2020.128

Muhammed O, and Çiğdem S. Ö. 2022. Equilibrium Studies for Dye Adsorption onto Red Clay. *Journal of Engineering and Natural Sciences* 3:2 (2022) 36-45. https://dergipark.org.tr/tr/pub/naturengs DOI: 10.46572/naturengs.1120218

Nayoon C, Yeongkyun S, Tae-Hyun K, Yuri P, and Yuhoon H. 2022. Adsorption behaviors of modified clays prepared with structurally different surfactants for anionic dyes removal. *Environmental Engineering Research* 2023; 28(2): 210076. DOI: https://doi.org/10.4491/eer.2022.076

Noroozi B., Soria G.A., Bahrami I.H. and Arami M. 2007 Equilibrium and kinetic adsorption study of a cationic dye by natural adsorbent-silkworm pupa *J. Hazard. Mater*. 139(1). 167- 174. Doi: 10.1016/j.jhazmat.2006.06.021.

Oguanobi N. C., Onu, C. E., and Onukwuli O. D. 2019. Adsorption of a dye (Crystal Violet) on acid modified non-conventional adsorbent. *Journal of Chemical Technology and Metallurgy*, 54 (1) 95-110.

Onu C. E., Oguanobi N. C., Okonkwo C. O., and Nnamdi-Bejie J. 2020. Application of Modified Agricultural Waste in the Adsorption of Bromocresol Green Dye. *Asian Journal of Chemical Sciences.* 7(1): 15-24. https://doi.org/10.9734/AJOCS/2020/v7i119011

Onu, C.E. and Nwabanne, J.T. 2014. "Application of Response Surface Methodology in Malachite green adsorption using Nteje clay". *Open Journal of Chemical Engineering and Science.* 1 (2) 19 – 33.

Paul E. D, and Mutsee T. 2021. Treated Clay Mineral as Adsorbent for the Removal of Heavy Metals from Aqueous Solution *Applied science and engineering progress* Vol 14, No 3 https://doi.org/10.14416/j.asep.2021.04.002

Popoola, T. J., Okoronkwo, A. E., Oluwasina, O. O., and Adebayo, M. A. 2021. Preparation, characterization, and application of a homemade graphene for the removal of Congo red from aqueous solutions. *Environ. Sci. Poll. Res*. 28, 52174–52187.

Reddy S.M.C., Sivaramakrishna L., and Reddy V.A. 2011. The use of an agricultural waste material, jujba seeds for the removal of anionic dye (Congo red) from aqueous medium. *Journal of Hazardous Materials* 203-204 (012) 118-127.

Redlich O, Peterson D.L. 1959. A useful adsorption isotherm. *Journal of Physical Chemistry*. 1959;63:1024.

Ritchie, A.G., 1977. Alternative to the Elovich equation for the kinetics of adsorption of gases on solids. J. Chem. Soc.,Faraday Trans. 1: Phys. Chem. Condens. Phases 73, 1650–1653.

Sabarish R, Jasila K, Aswathy J, Jyotishkumar P, Jaewoo L, Jyothi Mannekote S, Rajarathinam N, and Suchart S, (2022) Adsorption of anionic dye onto ZSM-5 zeolite-based bio membrane: Characterizations, kinetics and adsorption isotherm. *Journal of polymers and the environment*. https://doi.org/10.21203/rs.3.rs-1191111/v1

Salleh, M. A. M., Mahmoud, D. K., Karim, W. A., and Idris, A. 2011. Cationic and anionic dye adsorption by agricultural solid waste: a comparative review. *Desalination* 280 (1-3), 1-13.

Singha B. and Das S. 2013. Adsorptive removal of Cu (II) from aqueous solution and industrial effluent using natural and agricultural waste. *Colloids and surface* B, Vol 107, 2013, 77-106. Doi.org/10.1016/j.colsurfb.2013.01.060.

Spahn, H., and Schlunder, U. 1975. The scale-up of activated carbon columns for water purification based on results from batch test. I. Theoretical and experimental determination of adsorption rates of single organic solutes in batch test. Chem. Eng. Sci. 1975, 30, 529–537.

Srivastava, V. C., Mall, I. D., and Mishra, M. 2007. Adsorption thermodynamics and isosteric heat of adsorption of toxic metal ion onto bagasse fly ash (BFA) and rice husk ash (RHA), *Chem. Eng. J*.132, 267-278.

Temkin M., and Pyzhev V. 1940. Recent modifications to Langmuir isotherms. *ActaPhysiochim*. URSS 12, 217-222.

Venkatesh P.M., and Karthikeyan R. 2018. Comparative studies on modelling and optimization of hydrodynamic parameters on inverse fluidized bed reactor using ANN-GA and RSM. *Alexandria Engineering Journal* 57:3019–3032. https://doi.org/10.1016/j.aej.2018.05.002.

Wang G., He D., Fengchun Z.F., Hu J., Lee Y., Shi J., and Xu J. 2020 Extraction and purification of ustiloxin A from rice false smut balls by a combination of macroporous resin and high-speed countercurrent chromatography. *Food Production, Processing and Nutrition* 2:29 https://doi.org/10.1186/s43014-020-00043-9

Weber, W.J., and Morris, J.C. 1963 Kinetics of Adsorption on carbon from solutions. *Journal of the sanitary Engineering Division*, 89, 31-39.

Wu X., Hui K. N., Lee S. K., Zhou W., Chen R., Hwang D. H., Cho Y. R., and Son Y. G. 2012. Adsorption of basic yellow 87 from aqueous solution onto two different mesoporous adsorbents. *Chemical Engineering Journal* 180,91-98. doi:10.1016/j.cej.2011.11.009

Wu, C. H. 2007. Adsorption of reactive dye onto carbon nanotubes: equilibrium, kinetics and thermodynamics. *J. Hazard mater*. 144(1-2). 93-100. Doi:10.1016/j.jhazmat.2006.09.083.

Zhang X., Zhang J., Li W., Yang Y., Qin P., Zhang X., and Lu M. 2018. Magnetic graphene oxide nanocomposites as the adsorbent for extraction and pre-concentration of azo dyes in different food samples followed by high-performance liquid chromatography analysis. *Taylor & Francis Group* https://doi.org/10.1080/19440049.2018.1526415

Zhi L., Xiaohai H., Yi M., Bing G., Yiling S., Jianghui Z., Soon H. T. 2022. Eggplant biomass based porous carbon for fast and efficient dye adsorption from wastewater. *Industrial Crops and Products*.Volume 187, Part B, 1 November 2022, 115510 https://doi.org/10.1016/j.indcrop.2022.115510Get rights and content

Zineb El K., Jaouad B., Nouhaila F., Abdelali El M., Avni B., Zaki S., Hanae O., Farid K., Musaab D., Hiba-Allah N., Abdel-Rhman Z. G., Mohammed B., Amar H., and Nouredine EL M. 2023. Physicochemical Characterization of Clay and Study of Cationic Methylene Blue Dye Adsorption. *ACS Omega* 2023, 8, 43, 40848–40863. https://doi.org/10.1021/acsomega.3c06019.